experiments using the antigen peptide used for immunization (Supplemental data, Fig. S1). The anti-WNK1 antibody reacted with a band of ~250 kDa in several cell lines (Fig. 1). We subjected a lysate from HEK293 cells to immunoprecipitation with anti-WNK1 antibody and then immunoblotted the precipitates with anti-SPAK/OSR1 antibody. SPAK and OSR1 were found to coprecipitate with WNK1 (Fig. 1, *middle*). WNK1 was also detected with immunoprecipitates of SPAK and OSR1 from HEK293 cells or MDCK cells, indicating that these form an endogenous complex in living cells (Fig. 1, *left* and *right*).

SPAK and OSR1 bind to the cation-chloride transporters KCC3, NKCC1, and NKCC2 through a putative binding motif (R/K)FX(V/I) within the N-terminal tails of the transporters (22). In a yeast two-hybrid screen, SPAK was found to bind to WNK4, which contains a putative binding motif (23). A search of the amino acid sequences of human WNK1 revealed the presence of four putative SPAK-binding motifs (Fig. 2*A*). To further investigate the role of these motifs in WNK1 binding to STE20-related kinases, we co-expressed various forms of WNK1 with SPAK or OSR1 and performed co-immunoprecipitation experiments. Wild-type WNK1 was found to bind strongly to rat SPAK and mouse OSR1. WNK1(F1258A/F1869A) or WNK1(F1946A/F1958A), in which we mutated two of four SPAK-binding motifs by replacing the Phe residues with Ala, moderately deceased binding to SPAK/OSR1, and the additional mutations to the binding motifs of WNK1 showed gradually weak binding to SPAK/OSR1 depending on the number of mutations (Fig. 2*B*). These results suggested that WNK1 can associate with SPAK/OSR1 through four putative binding motifs.

WNK1 Phosphorylates the Evolutionary Conserved Serine Residues of SPAK and OSR1—To achieve specific and efficient phosphorylation of their substrates, many Ser/Thr protein kinases interact with the substrate via sites distinct from the phosphoacceptor sequence (28, 29). We first investigated whether SPAK and OSR1 are substrates of WNK1 kinase. By expression in bacteria, we produced a GST-tagged rat SPAK(KM) in which the Lys residue within subdomain II was replaced with Met. FLAG-tagged WNK1 was isolated from HEK293 cells and added to GST-SPAK(KM), and the mixture was analyzed by an *in vitro* kinase assay in the presence of [γ-^{32}P]ATP. In addition to WNK1 autophosphorylation, we observed that SPAK(KM) was phosphorylated in a time-dependent manner (Fig. 3*A*, *Wild type*). This phosphorylation was dependent on the kinase activity of WNK1 since phosphorylation was barely detectable when a kinase-dead form of WNK1 was used (Fig. 3*A*, *D368A*). To prove that SPAK is directly phosphorylated by WNK1 and not by putative kinases complexed with WNK1, we isolated several bacterially expressed WNK1 fragments tagged with GST. *In vitro* kinase analysis showed that the purified wild-type WNK1-(1–665) directly phosphorylated SPAK, whereas three forms of kinase-dead WNK1, K233M, D368A, or S382A, did not (Fig. 3*B*). Thus, our results indicated that the STE20-like kinase SPAK is a direct substrate of WNK1.

We next performed *in vitro* kinase assays using several deletion mutants of SPAK (Fig. 4*A*). GST-SPAK-(348–553) and GST-SPAK-(369–553), but not GST-SPAK-(400–553), were phosphorylated by WNK1, indicating that the WNK1 phosphorylation site(s) is located in the C-terminal regulatory region (369–400) of SPAK (Fig. 4*B*). Full-length GST-SPAK and GST-SPAK-(1–399) were also phosphorylated by WNK1, but the phosphorylation of these proteins is weaker than that of the C-terminal regulatory domain alone (Fig. 4*B*). It seems likely that the WNK1 phosphorylation site of SPAK is covered by the N-terminal region of SPAK including the kinase domain. There are four Ser/Thr residues, Ser-379, Ser-380, Thr-386, and Ser-394, within the 369–400 fragment of SPAK (Fig. 4*C*). To determine which residues are the site(s) of phosphorylation, various SPAK mutants were tested as substrates.

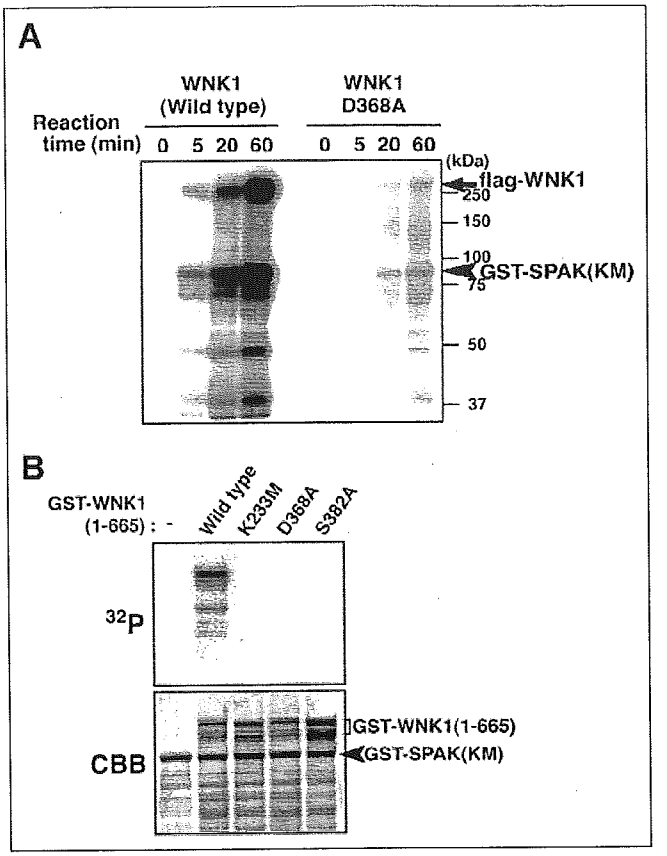

FIGURE 3. **WNK1 directly phosphorylates SPAK protein.** *A*, wild-type WNK1, but not kinase-dead WNK1 (WNK1(D368A)), mediates phosphorylation of SPAK. FLAG-tagged WNK1 and WNK1(D368A) isolated from transfected HEK293 cells were mixed with a GST-tagged kinase-dead form of SPAK (SPAK(KM)) and subjected to an *in vitro* kinase assay. The reaction was stopped at the indicated time points by the addition of SDS sample buffer. The protein complexes were separated by SDS-PAGE, and phosphorylated proteins were visualized by an image analyzer (BAS 2500). *B*, several bacterially produced GST-WNK1 fragments (wild type and three kinase-dead mutants (K233M, D368A and S382A)) and GST-SPAK(KM) were subjected to an *in vitro* kinase assay as indicated. Proteins were separated by SDS-PAGE and then visualized by Coomassie Brilliant Blue staining (*CBB*) and image analyzer (^{32}P).

The fragment 348–553(S380A) was not phosphorylated, indicating that Ser-380 is a major site of WNK1 phosphorylation (Fig. 4*B*). MS/MS analysis of tryptic peptides generated from phosphorylated recombinant SPAK proteins also indicated that Ser-380 is the site of phosphorylation (data not shown). Two small conserved regions were found in the C-terminal regions of SPAK and OSR1 and were named the PF1 and PF2 domains, respectively (Fig. 4*A*). Ser-380 of rat SPAK is located within the PF1 domain, and this Ser residue was highly conserved in other SPAK-related kinases, OSR1 and *Drosophila* Fray (Fig. 4*C*). We mutated the equivalent serine residue (Ser-325) in OSR1 to an Ala residue and examined phosphorylation by the WNK kinases. We found that both FLAG-WNK1 and FLAG-WNK4 were able to phosphorylate the full-length kinase-dead forms of SPAK and OSR1 but that mutation of the Ser residues to Ala of SPAK and OSR1 completely abolished or significantly reduced the phosphorylation (Fig. 4*D*). These data suggested that WNK1 phosphorylates these specific serine residues in SPAK-related kinases.

Ser-325 mutation of OSR1 Causes Its Activation—To examine the role that Ser phosphorylation of SPAK-related kinases plays in their regulation, we generated several mutants of OSR1. It has been recently reported that the N-terminal regulatory domain of p21-activated pro-

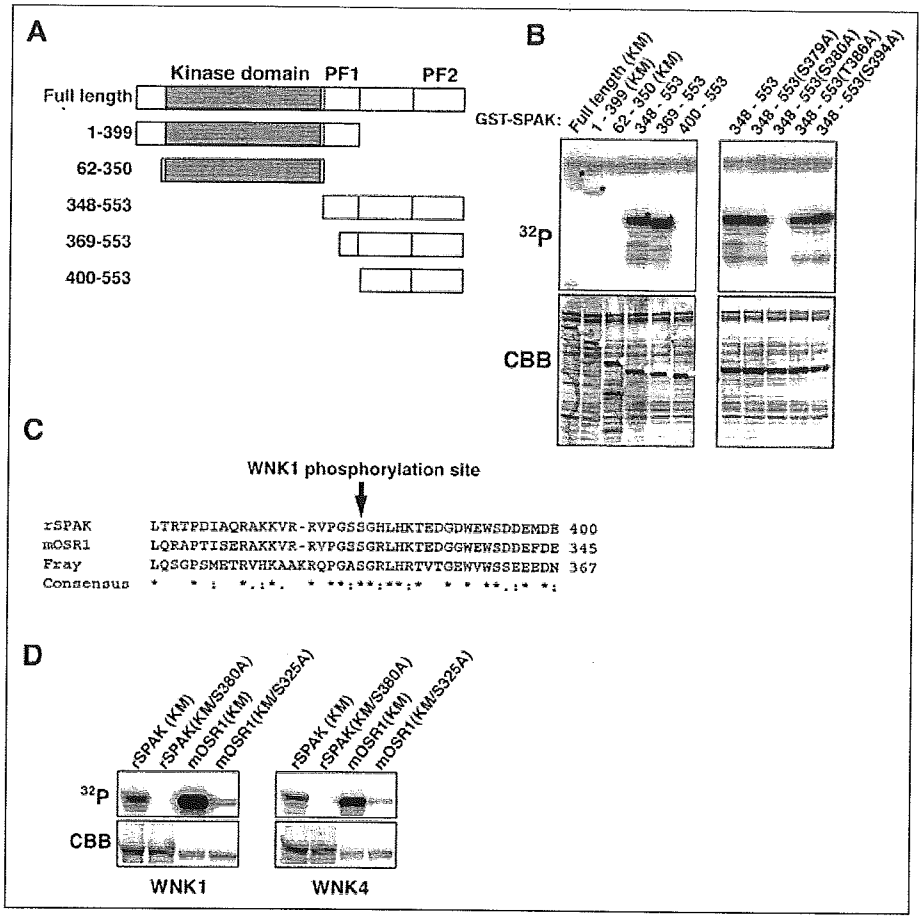

FIGURE 4. **WNK1 phosphorylates the conserved Ser residue in SPAK and OSR1.** *A*, schematic diagram of rat SPAK. Conserved domains among the SPAK-type STE20-related kinases are indicated as follows: kinase domain, PF1 domain (*PF1*), and PF2 domain (*PF2*). Fragments used in this study are also shown. *B*, GST-WNK1-(1–665) *in vitro* kinase assays were performed using the indicated GST-SPAK proteins as substrates and analyzed as in Fig. 3*B*. *Asterisks* indicate the sizes of the substrates. *CBB*, Coomassie Brilliant Blue staining. *C*, the amino acid sequence around the phosphorylation site of rat SPAK (*rSPAK*) is compared with that of mouse OSR1 (*mOSR1*) and *Drosophila* Fray by the ClustalW program. *Asterisks*, identical amino acids; *single* and *double dots*, weakly and strongly similar amino acids, respectively, determined by the criteria of the ClustalW program. *D*, FLAG-WNK1 (*left*) and FLAG-WNK4 (*right*) were isolated from transfected HEK293 cells and subjected to an *in vitro* kinase assay. GST fusion proteins of kinase-inactive SPAK(KM) or OSR1(KM) with or without the Ser to Ala point mutation were used as substrates and analyzed as in *panel B*.

tein kinase (PAK) is a physiological substrate of OSR1 (30). Wild-type GST-OSR1 exhibited a small amount of autophosphorylation, detectable by long exposure of the gel, but GST-OSR1KM showed no detectable activity (Fig. 5*A*). Since mutation of OSR1 Ser-325 to Asp mimics phosphorylation of this site, we generated GST-OSR1(S325D) and tested its activity. GST-OSR1(S325D) showed increased phosphorylation of GST-PAK3-(65–136), relative to wild-type OSR1 (Fig. 5*B*), indicating that the mutation Ser-325 to Asp of OSR1 causes constitutively activation of OSR1. Surprisingly, the mutation of the same site to Ala or Gly, which was expected to abolish phosphorylation, also resulted in causing constitutively activation of OSR1 (Fig. 5*B*, GST-OSR1(S325A), and data not shown). To further investigate the mechanisms of OSR1 activation, we examined several truncated forms of OSR1 (Fig. 5*C*). OSR1-(1–433) and OSR1-(1–344), truncated proteins lacking the PF2 domain, exhibited higher kinase activities than wild-type OSR1. In contrast, OSR1-(1–300), a truncated protein lacking both the PF1 and the PF2 domains, showed no detectable kinase activity (Fig. 5*D*). These results suggested that the PF1 domain of OSR1 is essential for kinase catalytic activity and that the PF2 domain is involved in regulating the catalytic activity.

SPAK and OSR1 Directly Phosphorylate the N-terminal Tail of Cation-Chloride Cotransporters—The activity of NKCC1 is regulated by phosphorylation/dephosphorylation, and examination of phosphorylation sites on NKCC1 revealed that three Thr residues in the N-terminal region, Thr-184, Thr-189, and Thr-202, are necessary for transport activity (19). NKCC2 and NCC are also members of the family of cation-chloride-coupled cotransporters, and the N-terminal regions of both cotransporters are conserved with that of NKCC1 (Fig. 6*A*). To test the possibility that SPAK and OSR1 are responsible for the phosphorylation of NKCC1, and also regulate NKCC2 and NCC, we prepared GST-tagged N-terminal fragments of each of these transporters. Both FLAG-SPAK and FLAG-OSR1 isolated from HEK293 cells were found to phosphorylate GST-NKCC2-(1–181), NKCC1-(1–289) and NCC-(1–138) (Fig. 6*B*). These proteins were also phosphorylated by GST-OSR1(S325D) *in vitro* (Fig. 6*C*), suggesting that phosphorylation was direct. The intensity of each phosphorylated band is comparable with or much higher than that observed using the GST-PAK3-(65–136) substrate, indicating that these cotransporters are good substrates for SPAK and OSR1. We next investigated the phosphorylation site(s) in the thiazide-sensitive transporter NCC using a series of mutations of the Ser/Thr residues that correspond to Thr-184, Thr-189, and Thr-202 of NKCC1. The T53A, T58A, and S71A mutants of NCC showed slightly reduced phosphorylation when compared with wild-type NCC. Moreover, there was no detectable increase in phosphorylation of the triple mutant, T53A/T58A/S71A (Fig. 6*D*). These results suggested that at least *in vitro*, SPAK/OSR1 directly phosphorylates the conserved Ser/Thr residues within the N-terminal regulatory region of NCC corresponding to shark NKCC1.

WNK1 and SPAK/OSR1 Are Activated by Low Cl^- Hypotonic Stress—Recent reports have shown that activation of shark and human Na-K-Cl cotransporter (NKCC1) by low Cl^- hypotonic stimulation is inhibited in cells expressing a dominant-negative mutant of SPAK and that the phosphorylation state of NKCC1 correlates with that of SPAK (24). Therefore, we tested whether hypotonic and low Cl^- conditions in cells

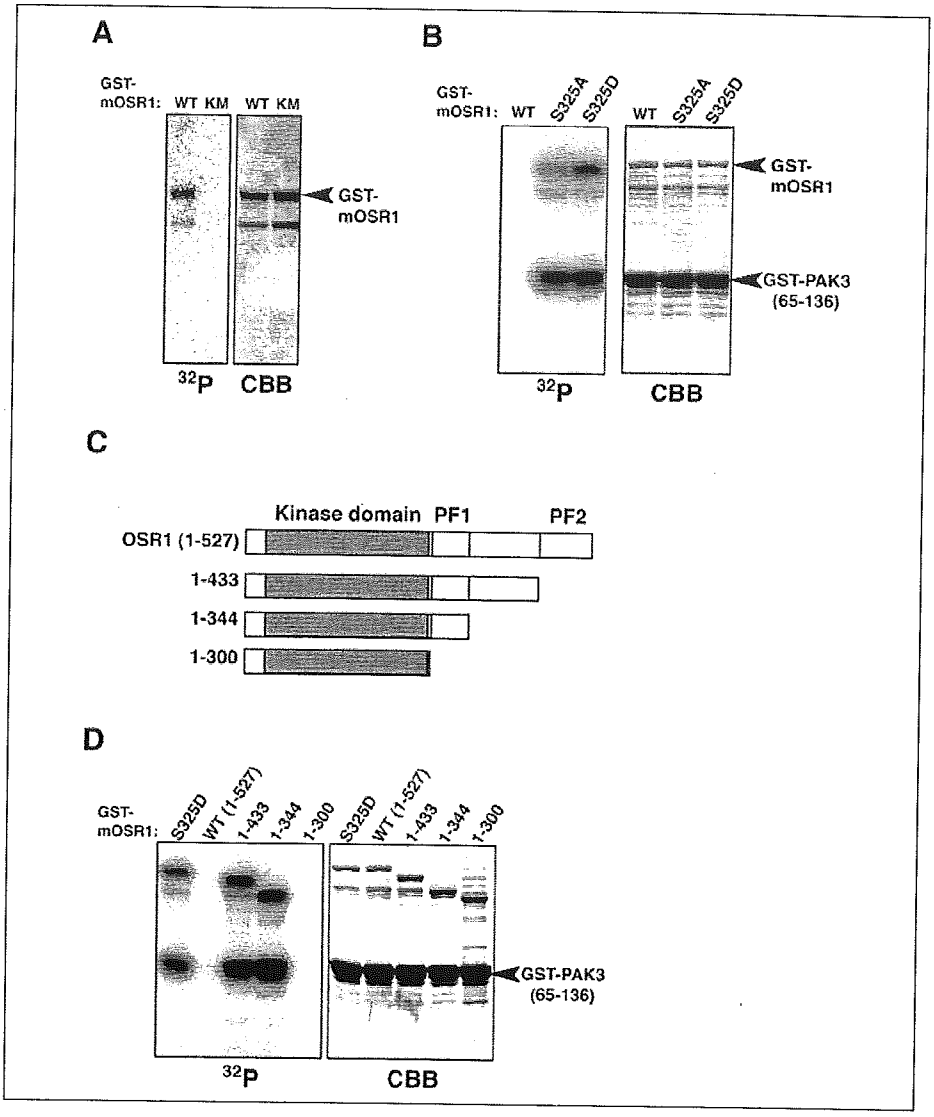

FIGURE 5. **Effects of WNK1 phosphorylation site modification on OSR1 activity *in vitro*.** *A*, kinase assays were performed with equal amounts of GST-tagged wild-type SPAK (*WT*) and kinase-dead form of OSR1(KM). *mOSR1*, mouse OSR1. *B*, GST-OSR1, GST-OSR1(S325A), and GST-OSR1(S325D) proteins were examined for their kinase activity toward GST-PAK3-(65–136). *C*, schematic diagram of mouse OSR1. Fragments used in *panel D* are also shown. *D*, the kinase activities of several OSR1 mutants were measured by *in vitro* kinase assay using GST-PAK3-(65–136) as a substrate. *CBB*, Coomassie Brilliant Blue staining.

lead to the activation of SPAK/OSR1. HEK293 cells were incubated with isotonic or low Cl^- hypotonic buffer, and endogenous WNK1 was immunoprecipitated and subjected to *in vitro* kinase assay using GST-SPAK-(348–553) as a substrate. We found that WNK1 kinase activity increased within 5 min and was sustained for at least 60 min by incubation in low Cl^- hypotonic conditions (Fig. 7*A*). We next examined the effect of low Cl^- hypotonic stimulation on phosphorylation and activation of SPAK/OSR1. When HEK293 cells transfected with an empty vector were incubated with hypotonic and low Cl^- buffer, SPAK/OSR1 autophosphorylation and kinase activity against GST-PAK3-(65–136) were increased (Fig. 7*B*). The phosphorylation of Ser-325 in OSR1 also occurred in cells under hypotonic and low Cl^- conditions. These results, together with those obtained *in vitro*, suggested that WNK1 functions as an activator for SPAK/OSR1 in response to Cl^- hypotonic stress in cells.

To clarify the role of the WNK/SPAK/OSR1 pathway in the phosphorylation of NCC, we performed a ^{32}P labeling experiment. Because we were unable to detect endogenous NCC in HEK293 cells or other cell lines by immunoblotting and immunostaining, T7-tagged mouse NCC was expressed in HEK293 cells. As shown in Fig. 7*C*, NCC was highly phosphorylated under low Cl^- hypotonic conditions. This result agreed well with the *in vitro* phosphorylation data and suggested that activation of the WNK1/SPAK/OSR1 pathway leads to the enhanced phosphorylation of NCC in cells.

DISCUSSION

In this study, we identified the STE20-like kinases, SPAK and OSR1, as targets of WNK1. WNK1 phosphorylates SPAK/OSR1 at a Ser residue within the PF1 domain, which is highly conserved among the mammalian SPAK/OSR1, *Drosophila* Fray, and *Caenorhabditis elegans* Y59A8B.23 gene products. WNK4 and WNK3 were also able to phosphorylate this residue (Fig. 2*F* and data not shown). In addition, *C. elegans* WNK1 phosphorylated the conserved Ser residue of the *C. elegans* SPAK/OSR1 homolog *in vitro*.[3] Thus, phosphorylation of SPAK/OSR1 by WNK kinase may be a common regulatory mechanism among species.

OSR1 mutants having point mutants in their PF1 domain or trunca-

[3] T. Moriguchi and H. Shibuya, unpublished data.

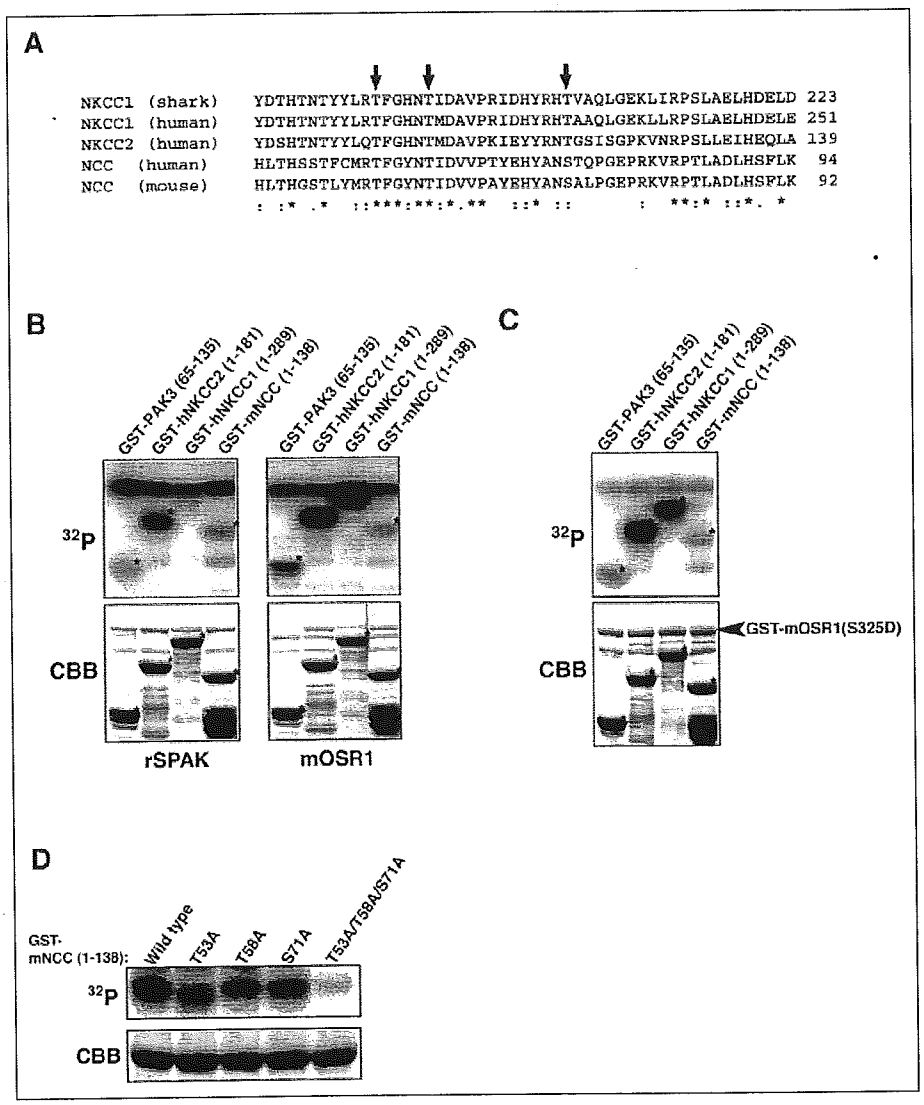

FIGURE 6. **N-terminal regulatory tail of cation-chloride-coupled cotransporter is phosphorylated by SPAK and OSR1.** *A*, alignment of the amino acid sequences of the regulatory regions in the N terminus of cation-chloride-coupled cotransporter, shark NKCC1, human NKCC1, human NKCC2, human NCC, and mouse NCC (*mNCC*). *Asterisks*, identical amino acids; *single* and *double dots*, weakly and strongly similar amino acids, respectively, were determined by the criteria of ClustalW program. *B*, T7-SAPK (*left*) or T7-OSR1 (*right*) isolated from HEK293 cells were assayed with GST-PAK3-(65–136), GST-hNKCC2-(1–181), GST-hNKCC1-(1–289), and GST-mNCC-(1–138) as substrates. Proteins were separated by SDS-PAGE and visualized by Coomassie Brilliant Blue (*CBB*) staining and an image analyzer (BAS 2500). *Asterisks* indicate the sizes of the substrates. *mOSR1*, mouse OSR1. *C*, GST-OSR1(S325D) was assayed for kinase activity as in *panel B*. *D*, GST-fusion proteins of NCC N-terminal fragments with the indicated Ser/Thr to Ala point mutations were used as substrates in GST-OSR1(S325D) kinase assays and analyzed as in *panel B*.

tion mutants lacking the PF2 domain exhibited higher kinase activities than wild-type OSR1 (Fig. 5). Moreover, a truncated mutant lacking the PF1 domain of OSR1 displayed no detectable kinase activity (Fig. 5*D*). It has been reported that many STE20-related kinases contain autoinhibitory domains and that removal of these regulatory domains results in a significant increase in kinase activity (31). Therefore, our results suggested that mutation of Ser-325 may cause constitutive activation of kinase activity due to conformational changes resulting from removal of the autoinhibitory PF2 domain rather than by an effect of negative charge. In the case of OSR1, the PF1 domain appeared to play an essential role in kinase catalytic activity, whereas the PF2 domain might be involved in regulating catalytic activity.

Mutation of the site in OSR1 that is phosphorylated by WNK1 resulted in enhanced OSR1 kinase activity, indicating that WNK1 plays an important role in the activation of SPAK and OSR1. However, *in vitro* phosphorylation of recombinant SPAK and OSR1 proteins by WNK1 or co-expression of SPAK and OSR1 with WNK1 in cells resulted in only weak activation of SPAK and OSR1 (data not shown). Therefore, WNK1 might not be the sole activator of SPAK and OSR1. The phosphorylation of multiple sites by several kinases has been shown to be required for the full activation of some kinases. For example, Akt is activated by phosphorylation on two residues, one in the activation loop of the kinase domain and the other located C-terminal to the catalytic domain (32). Phosphorylation of these sites in Akt is catalyzed by two kinases, 3-phosphoinositide-dependent kinase-1 (PDK1) and another tentatively called PDK2. Further studies will be needed to fully identify the kinase(s) that phosphorylates and activates SPAK/OSR1.

We also demonstrated that SPAK and OSR1 directly phosphorylate not only NKCC1 but also NKCC2 and NCC. These cation-chloride-cotransporters contain 12 transmembrane domains that are flanked by hydrophilic N- and C-terminal domains. It has been previously shown that three phosphorylation sites on the N terminus of shark NKCC1, Thr-189, Thr-184, and Thr-202, are necessary for full activation of transport activity (19). The sites of OSR1 phosphorylation in NCC include the three conserved Thr residues within the N-terminal regulatory region of the cation-chloride-coupled cotransporter family (Fig. 5), suggesting that WNK1 and SPAK/OSR1 could contribute to the regulation of transport activity. In fact, this hypothesis is supported by the recent finding that expression of both SPAK and WNK4 with NKCC1 in *Xenopus* oocytes results in a significant increase in NKCC1 activity (33). NCC, the mammalian thiazide-sensitive Na-Cl transporter, is expressed at the apical membrane of the distal convoluted

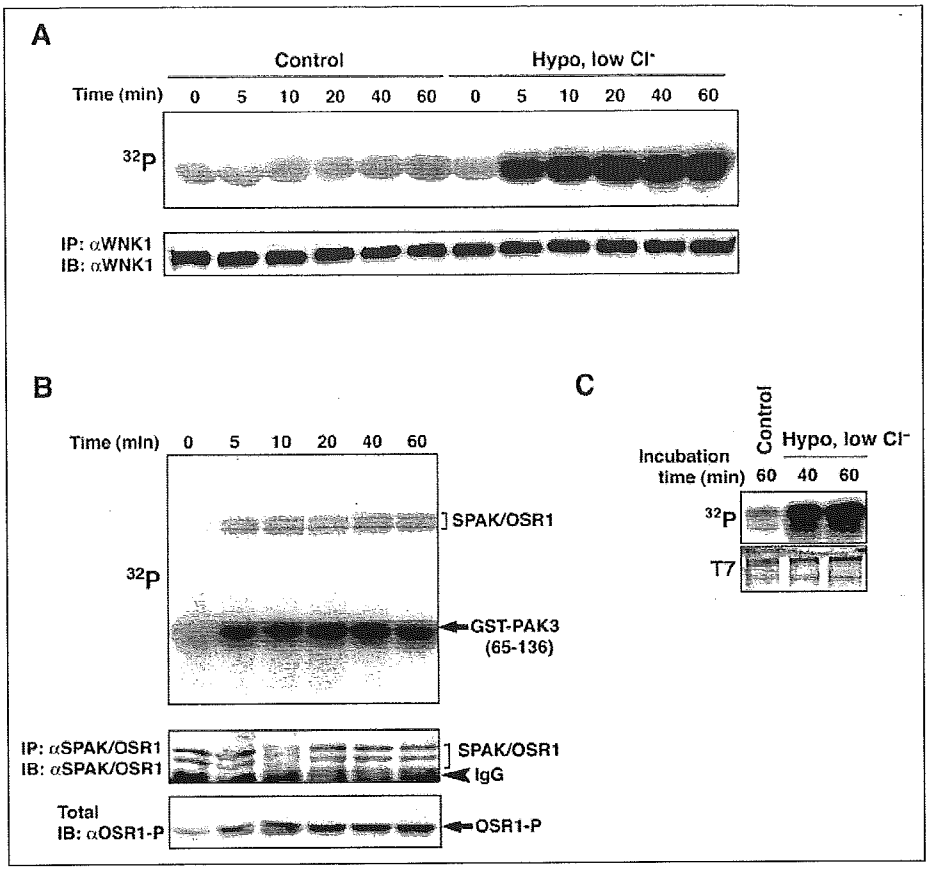

FIGURE 7. **Activation of WNK1 and SPAK/OSR1 by low Cl^- hypotonic stress.** *A*, HEK293 cells were incubated in isotonic buffer (*Control*) or low Cl^- hypotonic buffer (*Hypo, low* Cl^-) for the indicated times. The kinase activity of endogenous WNK1 was measured by an immune complex kinase assay using GST-SPAK-(348–553) as a substrate. The amount of immunoprecipitated WNK1 was detected by immunoblotting with the WNK1 antibody (immunoprecipitation (*IP*), αWNK1; immunoblotting (*IB*), αWNK1), and the phosphorylated GST-SPAK-(348–553) was detected by an image analyzer (BAS 2500) (^{32}P). *B*, HEK293 cells were incubated in low Cl^- hypotonic buffer for the indicated times. Endogenous SPAK/OSR1 was immunoprecipitated with the SPAK/OSR1 antibody, and subjected to an immune complex kinase assay using GST-PAK3-(65–136) as a substrate. The amount of SPAK/OSR1 in each immune complex was determined by immunoblotting (immunoprecipitation, αSPAK/OSR1; immunoblotting, αSPAK/OSR1). To monitor the Ser phosphorylation state of OSR1, lysates prepared from transfected cells were subjected to immunoblotting with the phospho-OSR1 antibody. Similar results were obtained in three different experiments. *C*, phosphorylation of T7-tagged NCC in HEK293cells. HEK293 cells were transfected with T7-NCC, metabolically labeled with [^{32}P]phosphate for 6 h, and then placed with isotonic buffer (*Control*) or low Cl^- hypotonic buffer for the indicated times prior to lysing. T7-NCC was immunoprecipitated using αT7 antibody.

tubule. Loss-of-function mutations in NCC have been shown to cause Gitelman syndrome, a disease characterized by salt wasting, hypokalemic metabolic alkalosis, and hypocalciuria. These clinical symptoms are the opposite of the symptoms observed in PHA II patients. The mutations in WNK1 associated with PHA II are intron deletions that cause increased expression of WNK1. Our findings supported the hypothesis that WNK1 phosphorylates and activates NCC, and this may provide a good explanation for pathogenesis of PHA II. However, the physiological relevance of these phosphorylation events to hypertension must be further evaluated by examining the regulation of NCC transport activity. In contrast to NCC, NKCC2, the bumetanide-sensitive cotransporter, is expressed in the apical membrane of the thick ascending limb of Henle's loop. Disruption of the *NKCC2* gene causes Bartter syndrome, an autosomal recessive disease characterized by metabolic alkalosis, hypokalemia, and hypercalciuria accompanied by a reduction in arterial blood pressure. Thus, it might be possible that activation of NKCC2 could account for hyperkalemia and hypertension in patients harboring *WNK1* mutations.

Tissue distribution reveals that WNK1 is widely expressed (1, 2). *WNK1*-deficient mice exhibit embryonic lethality, which indicates that WNK1 has important functions in many tissues, in addition to the kidney (34). NKCC1, SPAK, and OSR1 are also ubiquitously expressed and have multiple functions, such as regulation of cell volume, modulation of neuron excitability, AP-1-dependent gene expression, and regulation of the actin cytoskeleton (17, 30, 35). In this study, we identified a signaling pathway consisting of the PHA II disease-associated kinase WNK1 and the STE20-related kinases SPAK and OSR1, which culminates in the phosphorylation of several cotransporters. We hope that these findings will contribute to our understanding of the biological function for WNK1, not only in the pathogenesis of hypertension but also in other processes.

Acknowledgments—We thank T. Suganami and Y. Ogawa for valuable discussions, T. Akiyama for reagents, M. Lamphier for critical reading of the manuscript, and K. Nakamura and S. Tobiume for technical assistance.

Addendum—While this report was in preparation, a study describing WNK1/WNK4 phosphorylation of the same key serine residue, but also identifying an additional threonine residue within the activation loop, was published (36).

REFERENCES

1. Xu, B., English, J. M., Wilsbacher, J. L., Stippec, S., Goldsmith, E. J., and Cobb, M. H. (2000) *J. Biol. Chem.* **275**, 16795–16801
2. Verissimo, F., and Jordan, P. (2001) *Oncogene* **20**, 5562–5569
3. Min, X., Lee, B. H., Cobb, M. H., and Goldsmith, E. J. (2004) *Structure (Camb.)* **12**, 1303–1311
4. Wilson, F. H., Disse-Nicodeme, S., Choate, K. A., Ishikawa, K., Nelson-Williams, C., Desitter, I., Gunel, M., Milford, D. V., Lipkin, G. W., Achard, J. M., Feely, M. P., Dussol, B., Berland, Y., Unwin, R. J., Mayan, H., Simon, D. B., Farfel, Z., Jeunemaitre, X., and Lifton, R. P. (2001) *Science* **293**, 1107–1112
5. Wilson, F. H., Kahle, K. T., Sabath, E., Lalioti, M. D., Rapson, A. K., Hoover, R. S., Hebert, S. C., Gamba, G., and Lifton, R. P. (2003) *Proc. Natl. Acad. Sci. U. S. A.* **100**, 680–684
6. Yang, C. L., Angell, J., Mitchell, R., and Ellison, D. H. (2003) *J. Clin. Investig.* **111**, 1039–1045
7. Yang, S. S., Yamauchi, K., Rai, T., Hiyama, A., Sohara, E., Suzuki, T., Itoh, T., Suda, S., Sasaki, S., and Uchida, S. (2005) *Biochem. Biophys. Res. Commun.* **330**, 410–414
8. Kahle, K. T., Wilson, F. H., Leng, Q., Lalioti, M. D., O'Connell, A. D., Dong, K., Rapson, A. K., MacGregor, G. G., Giebisch, G., Hebert, S. C., and Lifton, R. P. (2003) *Nat. Genet.* **35**, 372–376
9. Kahle, K. T., Gimenez, I., Hassan, H., Wilson, F. H., Wong, R. D., Forbush, B., Aron-

son, P. S., and Lifton, R. P. (2004) *Proc. Natl. Acad. Sci. U. S. A.* **101,** 2064–2069
10. Kahle, K. T., Macgregor, G. G., Wilson, F. H., Van Hoek, A. N., Brown, D., Ardito, T., Kashgarian, M., Giebisch, G., Hebert, S. C., Boulpaep, E. L., and Lifton, R. P. (2004) *Proc. Natl. Acad. Sci. U. S. A.* **101,** 14877–14882
11. Yamauchi, K., Rai, T., Kobayashi, K., Sohara, E., Suzuki, T., Itoh, T., Suda, S., Hayama, A., Sasaki, S., and Uchida, S. (2004) *Proc. Natl. Acad. Sci. U. S. A.* **101,** 4690–4694
12. Lee, B. H., Min, X., Heise, C. J., Xu, B. E., Chen, S., Shu, H., Luby-Phelps, K., Goldsmith, E. J., and Cobb, M. H. (2004) *Mol. Cell* **15,** 741–751
13. Xu, B. E., Stippec, S., Lenertz, L., Lee, B. H., Zhang, W., Lee, Y. K., and Cobb, M. H. (2004) *J. Biol. Chem.* **279,** 7826–7831
14. Xu, B. E., Stippec, S., Chu, P. Y., Lazrak, A., Li, X. J., Lee, B. H., English, J. M., Ortega, B., Huang, C. L., and Cobb, M. H. (2005) *Proc. Natl. Acad. Sci. U. S. A.* **102,** 10315–10320
15. Xu, B. E., Stippec, S., Lazrak, A., Huang, C. L., and Cobb, M. H. (2005) *J. Biol. Chem.* **280,** 34218–34223
16. Hebert, S. C., Mount, D. B., and Gamba, G. (2004) *Pfluegers Arch. Eur. J. Physiol.* **447,** 580–593
17. Russell, J. M. (2000) *Physiol. Rev.* **80,** 211–276
18. Haas, M., and Forbush, B., III (2000) *Annu. Rev. Physiol.* **62,** 515–534
19. Darman, R. B., and Forbush, B. (2002) *J. Biol. Chem.* **277,** 37542–37550
20. Waldegger, S., Barth, P., Forrest, J. N., Jr., Greger, R., and Lang, F. (1998) *Pfluegers Arch. Eur. J. Physiol.* **436,** 575–580
21. Klein, J. D., Lamitina, S. T., and O'Neill, W. C. (1999) *Am. J. Physiol.* **277,** C425–C431
22. Piechotta, K., Lu, J., and Delpire, E. (2002) *J. Biol. Chem.* **277,** 50812–50819
23. Piechotta, K., Garbarini, N., England, R., and Delpire, E. (2003) *J. Biol. Chem.* **278,** 52848–52856
24. Dowd, B. F., and Forbush, B. (2003) *J. Biol. Chem.* **278,** 27347–27353
25. Okabe, T., Nakamura, T., Nishimura, Y. N., Kohu, K., Ohwada, S., Morishita, Y., and Akiyama, T. (2003) *J. Biol. Chem.* **278,** 9920–9927
26. James, P., Halladay, J., and Craig, E. A. (1996) *Genetics* **144,** 1425–1436
27. Natsume, T., Yamauchi, Y., Nakayama, H., Shinkawa, T., Yanagida, M., Takahashi, N., and Isobe, T. (2002) *Anal. Chem.* **74,** 4725–4733
28. Tanoue, T., Adachi, M., Moriguchi, T., and Nishida, E. (2000) *Nat. Cell Biol.* **2,** 110–116
29. Biondi, R. M., and Nebreda, A. R. (2003) *Biochem. J.* **372,** 1–13
30. Chen, W., Yazicioglu, M., and Cobb, M. H. (2004) *J. Biol. Chem.* **279,** 11129–11136
31. Dan, I., Watanabe, N. M., and Kusumi, A. (2001) *Trends Cell Biol.* **11,** 220–230
32. Brazil, D. P., Yang, Z. Z., and Hemmings, B. A. (2004) *Trends Biochem. Sci.* **29,** 233–242
33. Gagnon, K. B., England, R., and Delpire, E. (2005) *Am. J. Physiol.*, in press
34. Zambrowicz, B. P., Abuin, A., Ramirez-Solis, R., Richter, L. J., Piggott, J., Beltrandel-Rio, H., Buxton, E. C., Edwards, J., Finch, R. A., Friddle, C. J., Gupta, A., Hansen, G., Hu, Y., Huang, W., Jaing, C., Key, B. W., Jr., Kipp, P., Kohlhauff, B., Ma, Z. Q., Markesich, D., Payne, R., Potter, D. G., Qian, N., Shaw, J., Schrick, J., Shi, Z. Z., Sparks, M. J., Van Sligtenhorst, I., Vogel, P., Walke, W., Xu, N., Zhu, Q., Person, C., and Sands, A. T. (2003) *Proc. Natl. Acad. Sci. U. S. A.* **100,** 14109–14114
35. Li, Y., Hu, J., Vita, R., Sun, B., Tabata, H., and Altman, A. (2004) *EMBO J.* **23,** 1112–1122
36. Vitari, A. C., Deak, M., Morrice, N. A., and Alessi, D. R. (2005) *Biochem. J.* **391,** 17–24

Vol 437|27 October 2005|doi:10.1038/nature04106

nature

LETTERS

A heterodimeric complex that promotes the assembly of mammalian 20S proteasomes

Yuko Hirano[1], Klavs B. Hendil[2], Hideki Yashiroda[1], Shun-ichiro Iemura[3], Ryoichi Nagane[3], Yusaku Hioki[3], Tohru Natsume[3], Keiji Tanaka[1] & Shigeo Murata[1,4]

The 26S proteasome is a multisubunit protease responsible for regulated proteolysis in eukaryotic cells[1,2]. It comprises one catalytic 20S proteasome and two axially positioned 19S regulatory complexes[3]. The 20S proteasome is composed of 28 subunits arranged in a cylindrical particle as four heteroheptameric rings, $\alpha_{1-7}\beta_{1-7}\beta_{1-7}\alpha_{1-7}$ (refs 4, 5), but the mechanism responsible for the assembly of such a complex structure remains elusive. Here we report two chaperones, designated proteasome assembling chaperone-1 (PAC1) and PAC2, that are involved in the maturation of mammalian 20S proteasomes. PAC1 and PAC2 associate as heterodimers with proteasome precursors and are degraded after formation of the 20S proteasome is completed. Overexpression of PAC1 or PAC2 accelerates the formation of precursor proteasomes, whereas knockdown by short interfering RNA impairs it, resulting in poor maturation of 20S proteasomes. Furthermore, the PAC complex provides a scaffold for α-ring formation and keeps the α-rings competent for the subsequent formation of half-proteasomes. Thus, our results identify a mechanism for the correct assembly of 20S proteasomes.

It is presumed that assembly of 20S proteasomes starts by the spontaneous formation of α-rings[6–8]; however, the exact mechanism responsible for α-ring formation remains elusive. Seven β-subunits, some of which are in precursor forms, are arranged on the α-ring to form a complex named the 'half-proteasome', which consists of one α-ring, one β-ring and the chaperone protein Ump1. To complete maturation of the 20S proteasome, two half-proteasomes dimerize, the propeptides of β-subunits are removed and Ump1 is degraded[9–11]. This model is based mainly on studies in yeast. In mammals, POMP or Proteassemblin, a homologue of yeast Ump1 referred to here as human Ump1 (hUmp1), is also implicated in assembly of 20S proteasomes[15–17]. However, the biogenesis of 20S proteasomes remains largely elusive, especially in mammalian cells.

To identify proteins that interact with mammalian proteasomes, β1i subunits with a Flag tag were expressed in cells and anti-Flag immunoprecipitates were analysed by liquid chromatography coupled with tandem mass spectrometry[18]. We identified hUmp1 in addition to almost all of the subunits of 20S proteasomes and 19S regulatory complexes. We also identified two molecules with previously unknown relevance to proteasomes. One was Down syndrome critical region 2 (DSCR2), a small leucine-rich protein of 288 amino acids[19] that we have renamed PAC1. The other was a protein of 264 amino acids known as hepatocellular carcinoma associated gene 3 (HCCA3) (ref. 20), which we have renamed PAC2. Both PAC1 and PAC2 are ubiquitously expressed in mammals[19,20].

First, we confirmed that these molecules interact physically with proteasomes by transfecting Flag–PAC1 or Flag–PAC2 into HEK293T cells. The association increased on treatment of the cells with MG132, a proteasome inhibitor, in line with the increase in PAC1 and PAC2 expression (Supplementary Fig. 1a). Next, extracts of HeLa cells stably expressing Flag–PAC1 or Flag–PAC2 were fractionated by 8–32% glycerol gradient centrifugation. Both Flag–PAC1 and Flag–PAC2 were observed mainly in fractions containing sediments of precursor forms of proteasomes, as shown by the co-sedimentation of hUmp1, the unprocessed β1i (pro-β1i) subunit and α-subunits, and by the lack of chymotrypsin-like activity. Both Flag–PAC1 and Flag–PAC2 effectively co-precipitated with subunits from fraction 10 (Supplementary Fig. 1b, d). Moreover, even in fraction 16, which contained predominantly mature 20S proteasomes, they precipitated mainly with pro-β1i (Supplementary Fig. 1d), confirming that PAC1 and PAC2 associate specifically with precursor 20S proteasomes. Notably, the concentrations of precursor proteasomes were increased in both transfected cell lines (Supplementary Fig. 1c).

To examine the behaviour of endogenous PAC1 and PAC2 in detail, extracts from HEK293T cells were separated by lower density (4–24%) glycerol gradient centrifugation to resolve the precursor complexes. PAC1 and PAC2 were distributed mostly in the precursor fractions (Fig. 1a). Notably, the peaks of PAC1 and PAC2 were located in a fraction (fraction 12) lighter than that of the half-proteasomes (fraction 16), which contained hUmp1 and pro-β2. Moreover, the peaks of α5–α7 in precursor fractions were also located in fraction 12. Treatment with MG132 resulted in an accumulation of PAC1 and PAC2 in 20S proteasome fractions (Fig. 1a, right). The association of PAC1 and PAC2 with proteasomes was observed in fractions 12, 16 and 22 (Fig. 1b). When cells were treated with MG132, greater amounts of PAC1 and PAC2 were precipitated from fraction 22. Neither α4 nor α6 was associated with pro-β2 or hUmp1 in fraction 12. These results indicate that PAC1 and PAC2 form a complex with precursor 20S proteasomes before hUmp1 and the pro-β subunits are recruited, and suggest that PAC1 and PAC2 are chaperones for the maturation of 20S proteasomes and are released from or degraded by the newly assembled 20S proteasomes, analogous to the role of Ump1 in yeast[14].

To determine the composition of the peak of α-subunits that contained PAC1 and PAC2, fractions 12 and 16 were immunoprecipitated with antibodies against α6 and separated by two-dimensional polyacrylamide gel electrophoresis (2D-PAGE). Fraction 12 contained all seven α-subunits but no β-subunits, some of which were apparently detected in fraction 16 (Fig. 1c). Immunoblot analysis confirmed that all α-subunits except α1, which was difficult to distinguish by immunoblotting, were present in fraction 12 (Fig. 1d). The size of this complex (Fig. 1a), coupled with the absence of pro-β subunits or hUmp1 (Fig. 1a–c), means that it is

[1]Laboratory of Frontier Science, Core Technology and Research Center, Tokyo Metropolitan Institute of Medical Science, Bunkyo-ku, Tokyo 113-8613, Japan. [2]Institute of Molecular Biology and Physiology, University of Copenhagen, 13 Universitetsparken, DK 2100 Copenhagen, Denmark. [3]National Institute of Advanced Industrial Science and Technology, Biological Information Research Center, Kohtoh-ku, Tokyo 135-0064, Japan. [4]PRESTO, Japan Science and Technology Agency, Kawaguchi, Saitama 332-0012, Japan.

most probably a ring of all seven α-subunits, namely an α-ring. Immunoprecipitation in lower salt conditions showed that PAC1 and PAC2 are near-stoichiometric components of α-rings and that the association of PAC1 and PAC2 with α-subunits is salt labile (Fig. 1e, f). PAC1 was detected at a wide range of isoelectric point (pI) values, suggesting that it undergoes posttranslational modification (Fig. 1f). These results suggest that the PAC1–PAC2 complex and hUmp1 are distinct entities that work at different points in 20S proteasome assembly, and that PAC1 and PAC2 function as chaperone-like molecules at an earlier stage of 20S proteasome assembly relative to hUmp1.

Next, we characterized the interaction between PAC1 and PAC2. Coexpression of PAC1 and PAC2 in *Escherichia coli* and *in vitro* cotranscription–translation (IVTT) indicated that the two proteins bind directly (Supplementary Fig. 2a, b). Furthermore, PAC1 tagged with glutathione *S*-transferase (GST) pulled down PAC2 tagged with haemagglutinin A (HA) but not HA–PAC1, whereas GST–PAC2 pulled down HA–PAC1 but not HA–PAC2 *in vitro* (Supplementary Fig. 2b), indicating that PAC1 and PAC2 form hetero-oligomers but not homo-oligomers. No direct interaction between the PAC complex and hUmp1 was detected (Supplementary Fig. 2c). To determine the stoichiometry of the PAC complex, we coexpressed 3× Flag–PAC1 and 6× His–PAC2 in *E. coli* and purified the complex. PAC1 and PAC2 formed a complex at 1:1 stoichiometry with a relative molecular mass (M_r) corresponding to bovine serum albumin (67,000; Fig. 2a, b), indicating that the complex is a heterodimer.

To clarify further the nature of the PAC complex, we examined the half-lives of PAC1 and PAC2 by pulse-chase experiments. Both PAC1 and PAC2 turned over rapidly with similar half-lives of about 40 min (Fig. 2c). Treating the cells with MG132 markedly prolonged their half-lives, indicating that the PAC heterodimer is degraded by proteasomes. Because assembly of 20S proteasomes is complete within 1 h (ref. 21), the half-life of the PAC complex is consistent with the complex functioning as a chaperone for proteasome assembly and with its degradation on the completion of 20S proteasomes assembly.

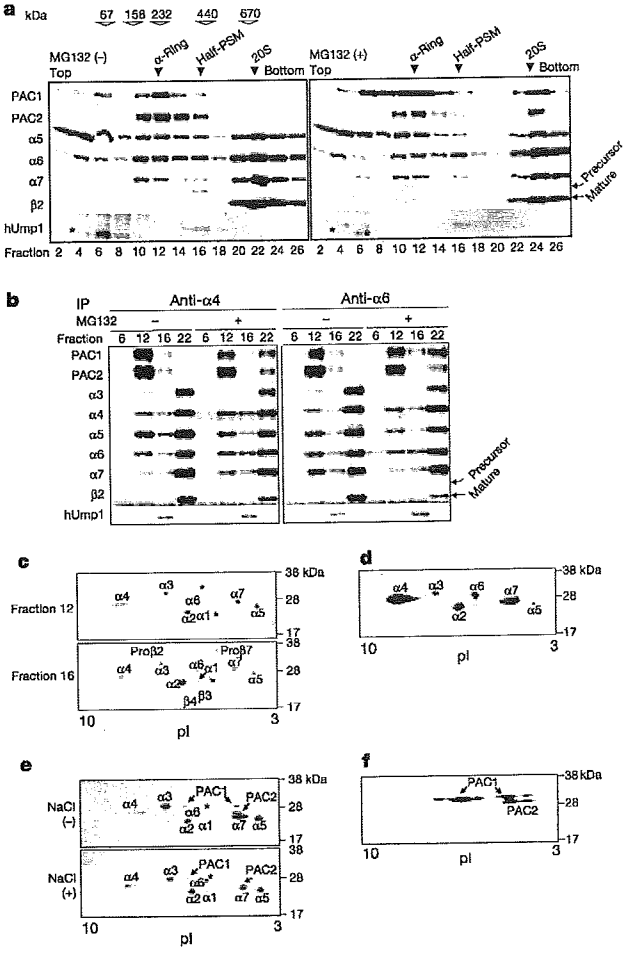

Figure 1 | PAC1 and PAC2 associate with precursor proteasomes. **a**, Glycerol gradient centrifugation (4–24%) of HEK293T cell extracts untreated or treated with MG132. Fractions were immunoblotted for the indicated proteins. Size markers and subcomplexes of proteasomes are indicated by open and filled arrowheads, respectively. Half-PSM indicates half-proteasomes. Asterisks indicate nonspecific bands. **b**, Fractions from **a** were immunoprecipitated with antibody against α4 or α6 and then subjected to immunoblotting. **c**–**f**, Fractions 12 (**c**–**f**) and 16 (**c**) from **a** were immunoprecipitated with beads conjugated to antibody against α6, washed with buffer A containing 150 mM (**c**, **d**), 0 mM or 50 mM (**e**, **f**) NaCl, eluted with glycine-HCl, and resolved by 2D-PAGE with silver (**c**) or Coomassie blue (**e**) staining. Asterisks denote unidentified spots. The top gel in **c** was immunoblotted with MCP231 and MCP34 antibodies against α-subunits and α4, respectively (**d**). The top gel in **e** was immunoblotted with antibodies against PAC1 and PAC2 (**f**). The non-uniformity of the spot intensity (**c**, **e**) may be due to a staining artefact because even in the half-proteasome fraction (fraction 16), which should contain all α-subunits in equal amounts, the spot intensities of α-subunits varied, resembling the pattern of fraction 12.

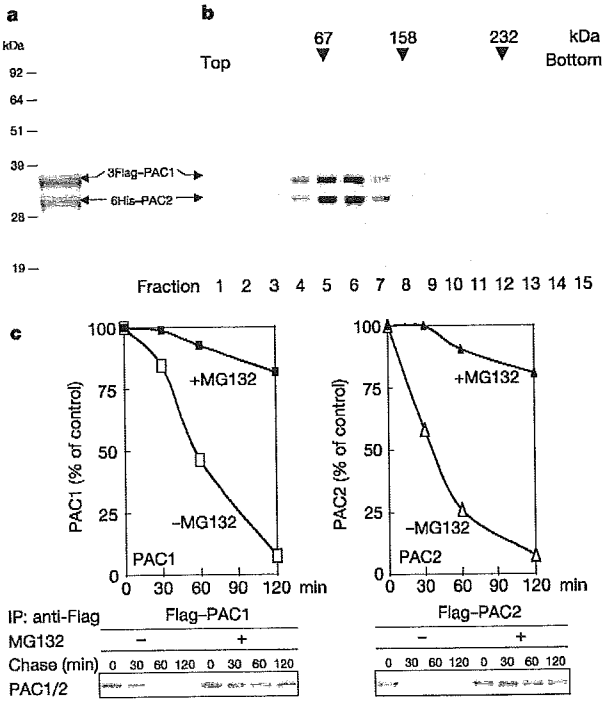

Figure 2 | The PAC1–PAC2 heterodimer is rapidly degraded by proteasomes. **a**, Coomassie blue staining of a copurified complex of 3× Flag–PAC1 and 6× His–PAC2 expressed in bacterial cells. **b**, The purified PAC complex in **a** was separated by 4–17% glycerol gradient centrifugation and subjected to SDS–PAGE with Coomassie staining. Arrowheads indicate size markers. **c**, Half-lives of PAC1 and PAC2. HeLa cells stably transfected with Flag–PAC1 or Flag–PAC2 were radiolabelled and chased in the presence or absence of MG132. Bottom panels show autoradiography; top panels show quantitative analysis of the bands.

To clarify the role of PAC1 and PAC2 in the assembly of the 20S proteasome *in vivo*, we used short interfering RNA (siRNA) to knock down the expression of PAC1 and PAC2. Knockdown of PAC1 resulted in loss of both PAC1 and PAC2 protein. Knockdown of PAC2 was also associated with a decrease in PAC1 protein (Fig. 3a), indicating that PAC1 and PAC2 are stable only when they form a heterodimer. Both PAC1- and PAC2-knockdown cells showed reduced proteolytic activity, as indicated by an assay of the antizyme-dependent degradation of ornithine decarboxylase (Supplementary Fig. 3a). Consequently, PAC-knockdown cells accumulated polyubiquitin-conjugated proteins, were sensitive to stress such as Cd^{2+}, and showed slow growth (Supplementary Fig. 3b–d).

We subjected the PAC-knockdown cells, as well as control and hUmp1-knockdown cells, to 4–24% glycerol gradient analysis. Notably, α-rings were hardly detected in either the PAC1- or the PAC2-knockdown cells (Fig. 3b). Instead, the α-subunits accumulated in fractions corresponding to half-proteasomes. This accumulation was not accompanied by an increase in pro-β2, pro-β5 or hUmp1, however, suggesting that the half-proteasomes were not normal. To confirm this notion, fraction 16 from the knockdown cells was immunoprecipitated with antibody against α6. Even though nearly equal amounts of α-subunits were loaded in the different samples, pro-β2, pro-β5 and hUmp1 were detected in much smaller amounts in PAC-knockdown cells (Fig. 3c), indicating that fraction 16 in PAC-knockdown cells contained mostly abnormally assembled α-subunits. This abnormal complex did not contain Rpt subunits, the components of 19S regulatory particles (Supplementary Fig. 3e, f), precluding the possibility that the mobility shift of α-subunits in PAC-knockdown cells was due to the premature association of α-subunits with Rpt subunits. On the basis of their sizes, these complexes are probably dimers of α-rings.

In hUmp1-knockdown cells, by contrast, we observed a marked reduction in 20S proteasomes but apparently normal α-rings and half-proteasomes, demonstrating the crucial role of hUmp1 in the dimerization of half-proteasomes. There was a strong increase in the free forms of some α-subunits in hUmp1-knockdown cells and a moderate increase in PAC-knockdown cells (Supplementary Fig. 3g). Assays of peptidase activities showed a significant reduction in activity of both the 20S and the 26S proteasome fractions in PAC-knockdown cells, although the effect of hUmp1 knockdown was more intense (Supplementary Fig. 3h). These data show definitively that the PAC complex has a pivotal role in the assembly of 20S proteasomes, specifically in keeping α-rings competent for the subsequent formation of half-proteasomes.

To elucidate the mechanism of PAC complex function, we tested the direct association of the complex with all of the subunits of 20S proteasomes. The PAC complex specifically interacted with α5 and α7, but not with other α-subunits or with any of the β-subunits *in vitro* (Supplementary Fig. 4a). Because Fig. 1a shows that the PAC1–PAC2 complex is found not only in α-ring fractions but also in lighter fractions, we considered whether it is involved in α-ring assembly. Immunoprecipitation with an antibody against Flag after the coexpression of all seven α-subunits, of which α5 was Flag-tagged, by IVTT showed that all α-subunits co-precipitated with Flag–α5 in larger amounts in the presence of the PAC complex than in its absence (Supplementary Fig. 4b). Immunoprecipitation with anti-Flag antibody after the coexpression of Flag–PAC1, PAC2 and α-subunits showed that PAC1 precipitated not only α5 and α7 but also all of the other α-subunits (Supplementary Fig. 4c), implying that it has a role in attracting α-subunits to each other.

We examined these interactions under more physiological conditions. Extracts of 293T cells that stably express Flag–PAC1 were separated by 4–24% glycerol gradient, and fractions corresponding to early α-subunit assembly intermediates and α-rings (fractions 8 and 12 in Fig. 1a, respectively) were immunoprecipitated with anti-Flag antibody and subjected to 2D-PAGE. PAC1 in fraction 12 co-precipitated all seven α-subunits, whereas PAC1 in fraction 8 co-precipitated several unidentified spots other than α-subunits, which made it difficult to identify α-subunits except for α5 and α7 by Coomassie staining (Fig. 4a, left). Immunoblot analysis showed that all α-subunits were present in the α-ring fraction, although α1 was difficult to distinguish (Fig. 4a, right), consistent with the findings in Fig. 1c. In contrast, PAC1 in fraction 8 co-precipitated a restricted set

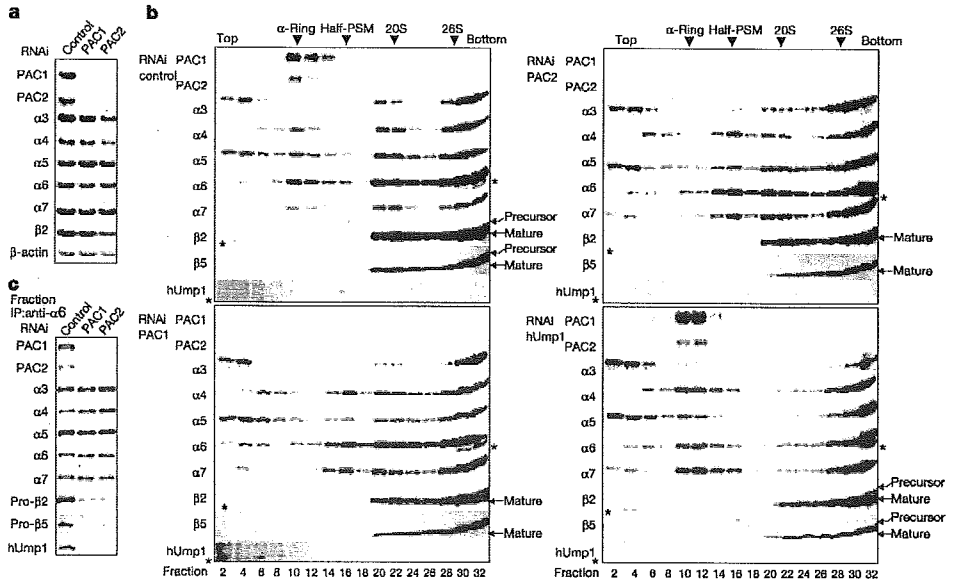

Figure 3 | siRNA-mediated knockdown of PAC1 and PAC2 impairs proteasome assembly. a–c, siRNA targeting PAC1 or PAC2, or control siRNA, was transfected into HEK293T cells. Knockdown of hUmp1 was also analysed in **b**. Whole-cell extracts (**a**), fractions separated by 4–24% glycerol gradient centrifugation (**b**), and immunoprecipitates obtained from fraction 16 in **b** with antibodies against α6 (**c**) were immunoblotted for the indicated proteins. Asterisks indicate nonspecific bands.

of α-subunits in which α3 and α4 were hardly detected. These results indicate that there is a hierarchy among α-subunits in their incorporation into α-rings, and that the PAC complex associates with the α-subunits before α-rings are complete, and functions as a scaffold for α-ring assembly.

Finally, we tested whether the complex of α-subunits in fraction 12 is a unique species. The affinity-purified complex from fraction 12 was subjected to native-PAGE. We found that the complex had a unique electrophoretic mobility (Fig. 4b). Moreover, the complex was eluted with a single sharp peak by anion-exchange chromatography (Fig. 4c). Thus, this complex is a unique species biochemically and is a genuine α-ring rather than a group of heterogeneous and incomplete α-ring precursors.

Our present work provides a model in which the chaperone complex PAC1–PAC2 mediates the formation of α-rings, keeps the rings competent for half-proteasome formation, and is required for proper proteasome maturation and cellular integrity (Fig. 4d). (See Supplementary Discussion for a more detailed description.)

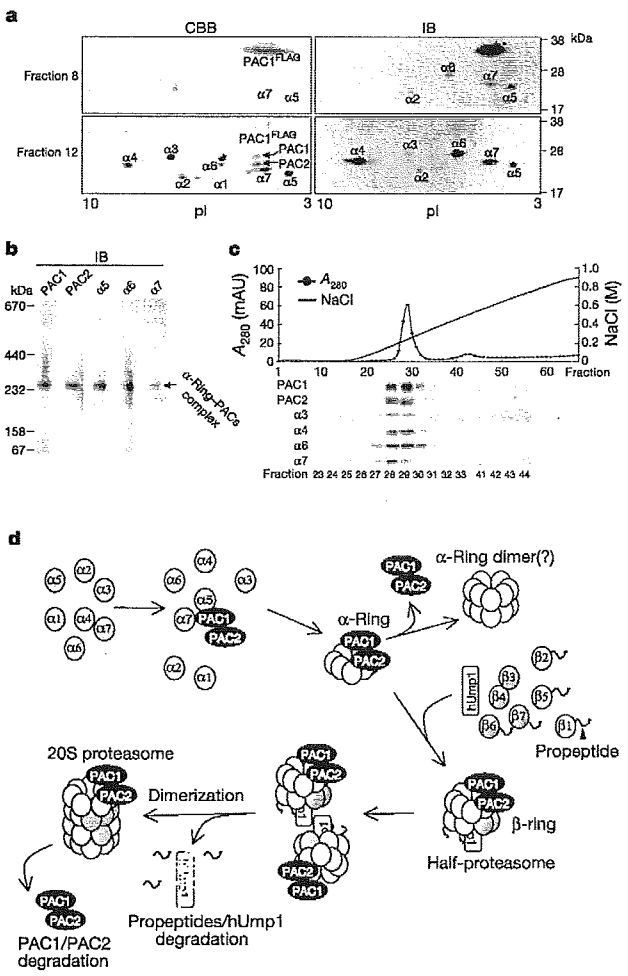

Figure 4 | PAC1–PAC2 provides a scaffold for α-ring formation. **a**, Extracts of HEK293T cells transfected with Flag–PAC1 were fractionated as in Fig. 1a. The Flag–PAC1 complexes from fractions 8 and 12 were purified with M2 agarose, resolved by 2D-PAGE and detected by Coomassie blue staining (left) or immunoblotting as in Fig. 1d (right). Asterisks denote unidentified spots. **b**, **c**, Purified Flag–PAC1 complex from fraction 12 was subjected to native-PAGE (**b**) or anion-exchange chromatography (**c**), followed by immunoblotting. **d**, Multistep model of the ordered assembly of mammalian 20S proteasomes. Some of the newly synthesized free α-subunits bind to the PAC1–PAC2 heterodimer, which provides a scaffold for α-ring formation, thereby suppressing the off-pathway aggregation of α-subunits and keeping α-rings competent for half-proteasome formation. Two half-proteasomes then dimerize, the β-subunits are processed and hUmp1 is degraded. The PAC1–PAC2 complex is subsequently degraded by the newly formed active 20S proteasomes.

METHODS

See Supplementary Methods for procedures used in the experiments in Supplementary Figs 1–4.

DNA constructs and cell culture. We synthesized cDNAs encoding PAC1, PAC2, hUmp1 and proteasome α- and β-subunits from total RNA isolated from HeLa cells using Superscript II (Invitrogen). PCR was carried out on the cDNA with Pyrobest DNA polymerase (Takara). All of the amplified fragments were cloned into pcDNA3.1 (Invitrogen) and sequenced for confirmation. For expression of GST fusion proteins, the cDNAs were subcloned into pGEX6P-1 (Amersham). Transfections of 293T cells were done with Fugene 6 (Roche). Stable transfections of HeLa cells or 293T cells were done with Lipofectamine 2000 (Invitrogen), and the cells were selected with 1 mg ml^{-1} of G418 or 5 μg ml^{-1} of puromycin, respectively. We used 20 μM MG132 (Peptide Institute) to inhibit proteasome activities 2 h before the cells were collected.

Protein extracts, immunological analysis and antibodies. Cells were lysed in ice-cold buffer A containing 50 mM Tris-HCl (pH 7.5), 0.5% (v/v) Nonidet P40, 1 mM dithiothreitol (DTT) and 2 mM ATP, and the extracts were clarified by centrifugation at 20,000*g* for 10 min at 4 °C. SDS–PAGE (12% gel or 4–12% gradient Bis-Tris gel; Invitrogen) and native-PAGE (3–8% gradient Tris-acetate gel; Invitrogen) were done in accordance with the manufacturer's instructions. The separated proteins were transferred onto polyvinylidene difluoride membrane and reacted with the indicated antibody. Development was done with Western Lighting reagent (Perkin Elmer). Polyclonal antibodies against hUmp1, PAC1 and PAC2 were raised in rabbits using a synthetic peptide (E_{115}DILNDPSQSE$_{125}$), and recombinant PAC1 and PAC2 protein, respectively. PAC1 and PAC2 were produced and purified as GST fusion proteins, and GST was removed by PreScission protease (Amersham).

Antibodies against proteasome α3 subunit (MCP257), α4 (MCP34), α5 (MCP196), α6 (MCP20), α7 (MCP72), β2 (MCP168) and α-subunits (MCP231, which reacts with all α-subunits except α4) were purchased from BioMol. Antibodies against β5 (P93250), β6 (P93199) and β1i were prepared as described[22]. We used antibodies against the Flag tag (Sigma) and β-actin (Chemicon), and horseradish peroxidase (HRP)-conjugated rabbit anti-mouse and goat anti-rabbit IgG (Jackson ImmunoResearch) for immunodetection. For immunoprecipitation of the Flag epitope, we used M2 agarose (Sigma). For immunoprecipitation of proteasomes, we used antibody MCP34 or MCP20 bound to protein G Sepharose (Amersham). In the experiments in Fig. 1e–f, we used MCP20 crosslinked to NHS-activated Sepharose (Amersham). These beads were added to the extracts, mixed under constant rotation for 2 h at 4 °C, washed four times with buffer A (except in the experiments in Fig. 1e–f), and boiled in SDS sample buffer, or eluted with 100 μg ml^{-1} of Flag peptides (Sigma) or with 0.2 M glycine-HCl (pH 2.8). Densitometric analysis was done with Image Gauge software (Fujifilm). 2D-PAGE was done as described[23].

Glycerol gradient analysis. Samples and molecular weight markers (Amersham) were fractionated by 4–17% (v/v), 4–24% (v/v) or 8–32% (v/v) linear glycerol density gradient centrifugation (22 h, 100,000*g*) as described[22].

Purification of PAC1–PAC2 complex. We coexpressed 3× FLAG–PAC1 and 6× His–PAC2 in *E. coli* using a pRSFDuet-1 vector (Novagen). The cell pellets were lysed in buffer B containing 20 mM sodium phosphate (pH 7.8), 500 mM NaCl and 1.0% Triton X-100, and sonicated. Ni-NTA Sepharose (Qiagen) was added to the extracts, which were then washed with buffer C containing 20 mM sodium phosphate (pH 6.0) and 500 mM NaCl, and eluted with buffer C plus 100 mM imidazole. The eluted products were further purified with M2 agarose and eluted with 100 μg ml^{-1} of Flag peptide (Sigma).

Pulse-chase experiments. Cells were incubated with methionine-free medium for 1 h, metabolically labelled with ^{35}S-methionine for 1 h, and then washed and chased for the indicated time. The cell lysates were immunoprecipitated with M2 agarose, fractionated by SDS–PAGE and visualized by autoradiography.

RNAi experiments. siRNAs targeting human PAC1, PAC2 and hUmp1 with the following 19-nucleotide sequences were designed by B-Bridge and synthesized by Dharmacon: PAC1, 5′-CCAGAAGCUUGAAGGGUUU-3′; PAC2, 5′-GCAUAAAUGCUGAAGUGUA-3′; hUmp1, a mixture of 5′-GCAAGUGG ACCUUUUGAAA-3′ and 5′-CCUGAGAAUUUCUGCUCAA-3′. Control siRNA (Non-specific Control Duplex VIII) was purchased from B-Bridge. Transfections of siRNAs into HEK293T cells were done with Lipofectamine

2000 at a final concentration of 50 nM in six-well dishes. The cells were analysed 72 h after transfection.

Assay of proteasome activity. Peptidase activity was measured by using a fluorescent peptide substrate, succinyl-Leu-Leu-Val-Tyr-7-amido-4-methyl-coumarin (Suc-LLVY-MCA), as described[22].

Chromatography. Anion-exchange chromatography was done with a Resource Q column (Amersham). Bound proteins were eluted with a salt gradient of 0–1 M NaCl in a buffer containing 50 mM Tris-HCl (pH 8.0), 1 mM DTT and 5% glycerol.

Received 27 June; accepted 2 August 2005.

1. Pickart, C. M. Mechanisms underlying ubiquitination. *Annu. Rev. Biochem.* 70, 503–533 (2001).
2. Glickman, M. H. & Ciechanover, A. The ubiquitin-proteasome proteolytic pathway: destruction for the sake of construction. *Physiol. Rev.* 82, 373–428 (2002).
3. Baumeister, W., Walz, J., Zühl, F. & Seemüller, E. The proteasome: paradigm of a self-compartmentalizing protease. *Cell* 92, 367–380 (1998).
4. Groll, M. *et al.* Structure of 20S proteasome from yeast at 2.4 Å resolution. *Nature* 386, 463–471 (1997).
5. Unno, M. *et al.* The structure of the mammalian 20S proteasome at 2.75 Å resolution. *Structure (Camb.)* 10, 609–618 (2002).
6. Zwickl, P., Kleinz, J. & Baumeister, W. Critical elements in proteasome assembly. *Nat. Struct. Biol.* 1, 765–770 (1994).
7. Gerards, W. L. *et al.* The human α-type proteasomal subunit HsC8 forms a double ringlike structure, but does not assemble into proteasome-like particles with the β-type subunits HsDelta or HsBPROS26. *J. Biol. Chem.* 272, 10080–10086 (1997).
8. Yao, Y. *et al.* α5 subunit in *Trypanosoma brucei* proteasome can self-assemble to form a cylinder of four stacked heptamer rings. *Biochem. J.* 344, 349–358 (1999).
9. Yang, Y., Früh, K., Ahn, K. & Peterson, P. A. *In vivo* assembly of the proteasomal complexes, implications for antigen processing. *J. Biol. Chem.* 270, 27687–27694 (1995).
10. Chen, P. & Hochstrasser, M. Autocatalytic subunit processing couples active site formation in the 20S proteasome to completion of assembly. *Cell* 86, 961–972 (1996).
11. Schmidtke, G. *et al.* Analysis of mammalian 20S proteasome biogenesis: the maturation of β-subunits is an ordered two-step mechanism involving autocatalysis. *EMBO J.* 15, 6887–6898 (1996).
12. Nandi, D., Woodward, E., Ginsburg, D. B. & Monaco, J. J. Intermediates in the formation of mouse 20S proteasomes: implications for the assembly of precursor β subunits. *EMBO J.* 16, 5363–5375 (1997).
13. Schmidtke, G., Schmidt, M. & Kloetzel, P. M. Maturation of mammalian 20 S proteasome: purification and characterization of 13 S and 16 S proteasome precursor complexes. *J. Mol. Biol.* 268, 95–106 (1997).
14. Ramos, P. C., Hockendorff, J., Johnson, E. S., Varshavsky, A. & Dohmen, R. J. Ump1p is required for proper maturation of the 20S proteasome and becomes its substrate upon completion of the assembly. *Cell* 92, 489–499 (1998).
15. Griffin, T. A., Slack, J. P., McCluskey, T. S., Monaco, J. J. & Colbert, R. A. Identification of proteassemblin, a mammalian homologue of the yeast protein, Ump1p, that is required for normal proteasome assembly. *Mol. Cell. Biol. Res. Commun.* 3, 212–217 (2000).
16. Witt, E. *et al.* Characterisation of the newly identified human Ump1 homologue POMP and analysis of LMP7(β5i) incorporation into 20 S proteasomes. *J. Mol. Biol.* 301, 1–9 (2000).
17. Burri, L. *et al.* Identification and characterization of a mammalian protein interacting with 20S proteasome precursors. *Proc. Natl Acad. Sci. USA* 97, 10348–10353 (2000).
18. Natsume, T. *et al.* A direct nanoflow liquid chromatography-tandem mass spectrometry system for interaction proteomics. *Anal. Chem.* 74, 4725–4733 (2002).
19. Vidal-Taboada, J. M. *et al.* Down syndrome critical region gene 2: expression during mouse development and in human cell lines indicates a function related to cell proliferation. *Biochem. Biophys. Res. Commun.* 272, 156–163 (2000).
20. Bahar, R. *et al.* Growth retardation, polyploidy, and multinucleation induced by Clast3, a novel cell cycle-regulated protein. *J. Biol. Chem.* 277, 40012–40019 (2002).
21. Ahn, K. *et al. In vivo* characterization of the proteasome regulator PA28. *J. Biol. Chem.* 271, 18237–18242 (1996).
22. Tanahashi, N. *et al.* Hybrid proteasomes. Induction by interferon-γ and contribution to ATP-dependent proteolysis. *J. Biol. Chem.* 275, 14336–14445 (2000).
23. Murata, S. *et al.* Immunoproteasome assembly and antigen presentation in mice lacking both PA28α and PA28β. *EMBO J.* 20, 5898–5907 (2001).

Supplementary Information is linked to the online version of the paper at www.nature.com/nature.

Acknowledgements We thank Y. Murakami for the ornithine decarboxylase degradation assay system, K. Furuyama for technical support, and D. Finley for comments on the manuscript. This work was supported by grants from the Japanese Science and Technology Agency (to S.M.), the Ministry of Education, Science and Culture of Japan (to S.M. and K.T.) and the New Energy and Industrial Technology Development Organization (to T.N.). Y.H. was supported by the Japanese Society for the Promotion of Science.

Author Information The sequences for human PAC1 and PAC2 have been deposited in GenBank under accession numbers BR000236 and BR000237, respectively. Reprints and permissions information is available at npg.nature.com/reprintsandpermissions. The authors declare no competing financial interests. Correspondence and requests for materials should be addressed to S.M. (smurata@rinshoken.or.jp) or K.T. (tanakak@rinshoken.or.jp).

The EMBO Journal (2006) 25, 554–564 | © 2006 European Molecular Biology Organization | All Rights Reserved 0261-4189/06
www.embojournal.org

THE EMBO JOURNAL

A novel ubiquitin-binding protein ZNF216 functioning in muscle atrophy

Akinori Hishiya[1,2], Shun-ichiro Iemura[3], Tohru Natsume[3], Shinichi Takayama[2], Kyoji Ikeda[1] and Ken Watanabe[1,*]

[1]Department of Bone & Joint Disease, National Center for Geriatrics & Gerontology (NCGG), Obu, Aichi, Japan, [2]Program of Molecular Chaperone Biology, Department of Radiology, Medical College of Georgia, Augusta, GA, USA and [3]Japan Biological Information Research Center (JBIRC), National Institute of Advanced Industrial Science & Technology (AIST), Tokyo, Japan

The ubiquitin–proteasome system (UPS) is critical for specific degradation of cellular proteins and plays a pivotal role on protein breakdown in muscle atrophy. Here, we show that ZNF216 directly binds polyubiquitin chains through its N-terminal A20-type zinc-finger domain and associates with the 26S proteasome. ZNF216 was colocalized with the aggresome, which contains ubiquitinylated proteins and other UPS components. Expression of *Znf216* was increased in both denervation- and fasting-induced muscle atrophy and upregulated by expression of constitutively active FOXO, a master regulator of muscle atrophy. Mice deficient in *Znf216* exhibited resistance to denervation-induced atrophy, and ubiquitinylated proteins markedly accumulated in neurectomized muscle compared to wild-type mice. These data suggest that ZNF216 functions in protein degradation via the UPS and plays a crucial role in muscle atrophy.

The EMBO Journal (2006) **25**, 554–564. doi:10.1038/sj.emboj.7600945; Published online 19 January 2006
Subject Categories: proteins; molecular biology of disease
Keywords: aggresome; muscular atrophy; proteasome; ubiquitin; zinc-finger protein

Introduction

The ubiquitin–proteasome system (UPS) is one of the major protein degradation pathways in eukaryotic cells. The UPS plays key regulatory roles in many cellular processes, including cell cycle control, the regulation of transcription and protein quality control (Hershko and Ciechanover, 1998; Pickart and Cohen, 2004). Aberrations of this system lead to many forms of pathogenesis, such as malignancies, neurodegenerative disease and inflammatory response (Glickman and Ciechanover, 2002). The UPS includes sequential, multistep reactions: ubiquitin-conjugation of target proteins by E1, E2 and E3 enzymes, recognition of ubiquitinylated proteins by ubiquitin-binding proteins or 19S subunits of proteasome and proteolysis in the proteasome.

Many catabolic conditions, such as low-insulin state, hyperthyroidism, sepsis and cancer cachexia lead to enhancement of protein breakdown in skeletal muscle known as muscle atrophy (Mitch and Goldberg, 1996; Lecker *et al*, 1999). In muscle atrophy, the UPS plays a pivotal role in protein breakdown (Price *et al*, 1996; Tawa *et al*, 1997). Several studies indicate that mRNAs encoding UPS components are increased in atrophying muscle (Medina *et al*, 1991; Wing and Goldberg, 1993; Bailey *et al*, 1996; Price *et al*, 1996; Jagoe *et al*, 2002). In particular, the E3 ubiquitin ligases MAFbx/Atrogin-1 and MuRF-1 (muscle RING finger 1) are known to be markers of muscle atrophy (Bodine *et al*, 2001; Gomes *et al*, 2001). Both are induced in multiple models of muscle atrophy including immobilization, denervation and hindlimb suspension, and mice deficient in either gene are resistant to denervation-induced muscle atrophy (Bodine *et al*, 2001). Goldberg and co-workers proposed that atrophy-related genes, whose expression is induced in multiple types of muscle atrophy, are called 'atrogenes' (Sandri *et al*, 2004). Recently, it was demonstrated that the IGF-I/PI3K/Akt pathway is an important regulator of muscle mass in muscle hypertrophy and atrophy (Sacheck *et al*, 2004; Sandri *et al*, 2004; Stitt *et al*, 2004). In that case, the transcription factor FOXO plays a pivotal role in activating atrogenes such as MAFbx/Atrogin-1 (Gomes *et al*, 2001).

Although many UPS players such as E3 ligases have been characterized, the mechanism of how ubiquitinylated proteins are delivered to the proteasome have not been fully elucidated. A component of 19S proteasome, Rpn10/S5a, recognizes the ubiquitinylated proteins (Young *et al*, 1998; Wilkinson *et al*, 2000). It has been shown that yeast proteins, Rad23p and Dsk2p, bind to ubiquitinylated substrates and to the 26S proteasome through their UBA and Ubl domains, respectively, thereby functioning as shuttle proteins that present polyubiquitinylated proteins to the proteasome (Chen *et al*, 2001; Funakoshi *et al*, 2002; Elsasser and Finley, 2005). Loss-of-function of shuttle proteins results in abnormal accumulation of polyubiquitinylated proteins (Lambertson *et al*, 1999; Saeki *et al*, 2002). However, yeast can survive when both *RAD23* and *DSK2* genes are mutated, suggesting that other mechanisms or molecule(s) possessing a shuttle function exist (Saeki *et al*, 2002). Here, we show that ZNF216, a novel ubiquitin-binding protein containing an A20-type zinc-finger, is such a factor. *Znf216* expression is upregulated in skeletal muscle in experimental models of muscle atrophy, and *Znf216*-deficient mice exhibit resistance to muscle atrophy accompanied by abnormal accumulation of polyubiquitinylated proteins in skeletal muscle. Our findings suggest that ZNF216, with its potential function of anchoring ubiquitinylated proteins to the proteasome, plays a critical role in degrading muscle proteins.

*Corresponding author. Department of Bone & Joint Disease, National Center for Geriatrics & Gerontology (NCGG), Obu, Aichi 474-8522, Japan. Tel.: +81 562 46 2311; Fax: +81 562 44 6595; E-mail: kwatanab@nils.go.jp

Received: 6 June 2005; accepted: 14 December 2005; published online: 19 January 2006

Results

ZNF216 directly binds to polyubiquitin

We have identified a gene, *Znf216* (*Za20d2*, Mouse Genome Informatics), encoding an A20 zinc-finger (Znf-A20) motif-containing protein, as a RANKL-induced gene upregulated upon osteoclast formation using a microarray technique (Hishiya *et al*, 2005). *Znf216* was originally identified as a candidate gene for hearing loss and is expressed in cochlear and skeletal muscle (Scott *et al*, 1998; Huang *et al*, 2004). To determine the function of ZNF216, we searched for molecules that associate with ZNF216 using yeast two-hybrid screening and isolated several clones encoding a gene for polyubiquitin C. To determine whether ZNF216 interacts with ubiquitin in mammalian cells, we transfected HEK293 cells with an expression vector for FLAG-tagged ZNF216 and HA-tagged ubiquitin and performed co-immunoprecipitation experiments. ZNF216 possesses A20-type (amino acids 11–35) and AN1-type (amino acids 154–191) zinc-finger domains at its N- and C-termini, respectively (Figure 1A). Endogenous ubiquitinylated proteins, which appear as smears, were co-immunoprecipitated with FLAG-tagged ZNF216 (Figure 1B). Notably, N-terminal deletion (ΔN; amino acids 36–213) or point mutants (M1 and M3) of the A20-type zinc-finger (ZnF-A20) domain abolished ubiquitin-binding ability of ZNF216, indicating that the ZnF-A20 domain is indispensable for binding to ubiquitin (Figures 1A and B). Whereas in non-denaturing conditions, ubiquitinylated molecules were present with FLAG-tagged ZNF216, these molecules completely disappear from immunoprecipitates following heat denaturation, which abolishes noncovalent protein–protein interactions (Figure 1C), suggesting that ZNF216 associates with ubiquitinylated proteins rather than being ubiquitinylated itself. Next, to determine whether ZNF216 binds to ubiquitin directly, we performed GST pull-down assays using GST-ZNF216 fusion proteins (Figure 1D) and purified polyubiquitin. As shown in Figure 1E, GST-ZNF216 but not GST bound to polyubiquitin chains. As expected, binding of ZNF216 to polyubiquitin chains was completely abolished by a point mutation in the ZnF-A20 domain (M1, Figure 1E). Furthermore, a GST fusion protein containing only the ZnF-A20 domain (amino acids 2–60) could bind to polyubiquitin chains, suggesting that ZNF216 directly binds to polyubiquitin chains, and that the ZnF-A20 domain is required for binding to polyubiquitin. As for other ZnF-A20 containing proteins, AWP1 (ZA20D3) also possessed polyubiquitin-binding activity but the ZnF-A20 domain(s) of Rabex-5 (Horiuchi *et al*, 1997) and A20/TNFAIP3 (Opipari *et al*, 1990) proteins did not (Supplementary Figure S1).

ZNF216 associates with the 26S proteasome

We also identified molecules associating with ZNF216 by proteomic analysis of complexes formed with FLAG-tagged ZNF216. Molecules expressed in HEK293 cells and that co-immunoprecipitated with FLAG-tagged ZNF216 were analyzed by tandem mass spectrometry. By this analysis, every subunit of the 26S proteasome complex was identified as associating with FLAG-tagged ZNF216 (data not shown). To identify the region of ZNF216 required for association with the 26S proteasome, lysates of cells expressing either FLAG-tagged ZNF216 or its mutants were immunoprecipitated with anti-FLAG antibody. Co-precipitation of proteasomal components was monitored by immunoblotting using an antibody against Rpn7p (S10a), a non-ATPase subunit of the 19S regulatory subunit. As shown in Figure 2A, this protein efficiently co-precipitated with FLAG-tagged ZNF216. The interaction was also observed with truncated or point mutants of ZnF-A20 (ΔN or M1), indicating that ubiquitin-binding ability is dispensable for association with the 26S proteasome. To determine whether endogenous ZNF216 proteins are also associated with the 26S proteasome, we performed a GST pull-down assay using the ubiquitin-like (Ubl) domain of hHR23B, a human homologue of Rad23, which is known to bind to the 26S proteasome. As shown in Figure 2B, GST-Ubl but not GST was pulled down with the endogenous 26S proteasome. Endogenous ZNF216 was also detected in the GST-Ubl/26S proteasome complex (upper panels, Figure 2B). Furthermore, purified recombinant ZNF216 did not bind to GST-Ubl (lower panel, Figure 2B), suggesting that endogenous ZNF216 is not directly bound to the Ubl domain but associates with the 26S proteasome.

Colocalization with the aggresome

Next, we determined the subcellular localization of ZNF216. Indirect immunofluorescence of ZNF216 expressed in COS-7 cells showed that the protein was largely cytoplasmic but was seen to a lesser extent in the nucleus (Figure 3A). Aggresomes, which are insoluble aggregates of ubiquitinylated proteins complexed with the proteasome and induced by treatment with proteasome inhibitors, are known to mimic inclusions seen in pathogenic UPS disorders (Johnston *et al*, 1998; Kopito, 2000; Lelouard *et al*, 2002). As shown in Figures 3D–H, ZNF216 proteins were colocalized with aggresomes induced by treatment with the proteasome inhibitor MG132. ZNF216 itself was not ubiquitinylated as shown in Figure 1C.

Induction of ZNF216 expression upon muscle atrophy

Biochemical and cell biological evidence presented here strongly suggests that ZNF216 functions in the UPS. In skeletal muscle, it is generally accepted that the UPS plays a critical role in muscular atrophy, and expression of atrophy-related genes including those encoding UPS components is induced in atrophying muscle (Jagoe *et al*, 2002; Lecker *et al*, 2004). As *Znf216* was predominantly expressed in brain and skeletal muscle (Scott *et al*, 1998), we investigated the relationship between ZNF216 and muscle atrophy. To determine whether *Znf216* expression is induced during muscle atrophy, an *in vitro* model of muscle atrophy was utilized. It has been reported that addition of dexamethasone to cultures of differentiated C2C12 myotubes causes formation of myotubes exhibiting signs of atrophy, including a reduction in myotube diameter (Stitt *et al*, 2004). Such treatment dramatically induced expression of *Znf216* (Figure 4A).

Next, expression of *Znf216* was determined in *in vivo* experimental models of muscle atrophy. Mice that undergo fasting for 2 days show significant decreases in body weight, as well as in the mass of the gastrocnemius muscles (data not shown). In this model, fasting for 2 days results in dramatic increases in *Znf216* mRNA (Figure 4B) and protein (Supplementary Figure S3) in muscle. Although there were differences in induction patterns of two differently sized transcripts of Znf216 by atrophy-inducting stimuli, both transcripts encode the same protein (Supplementary Figures

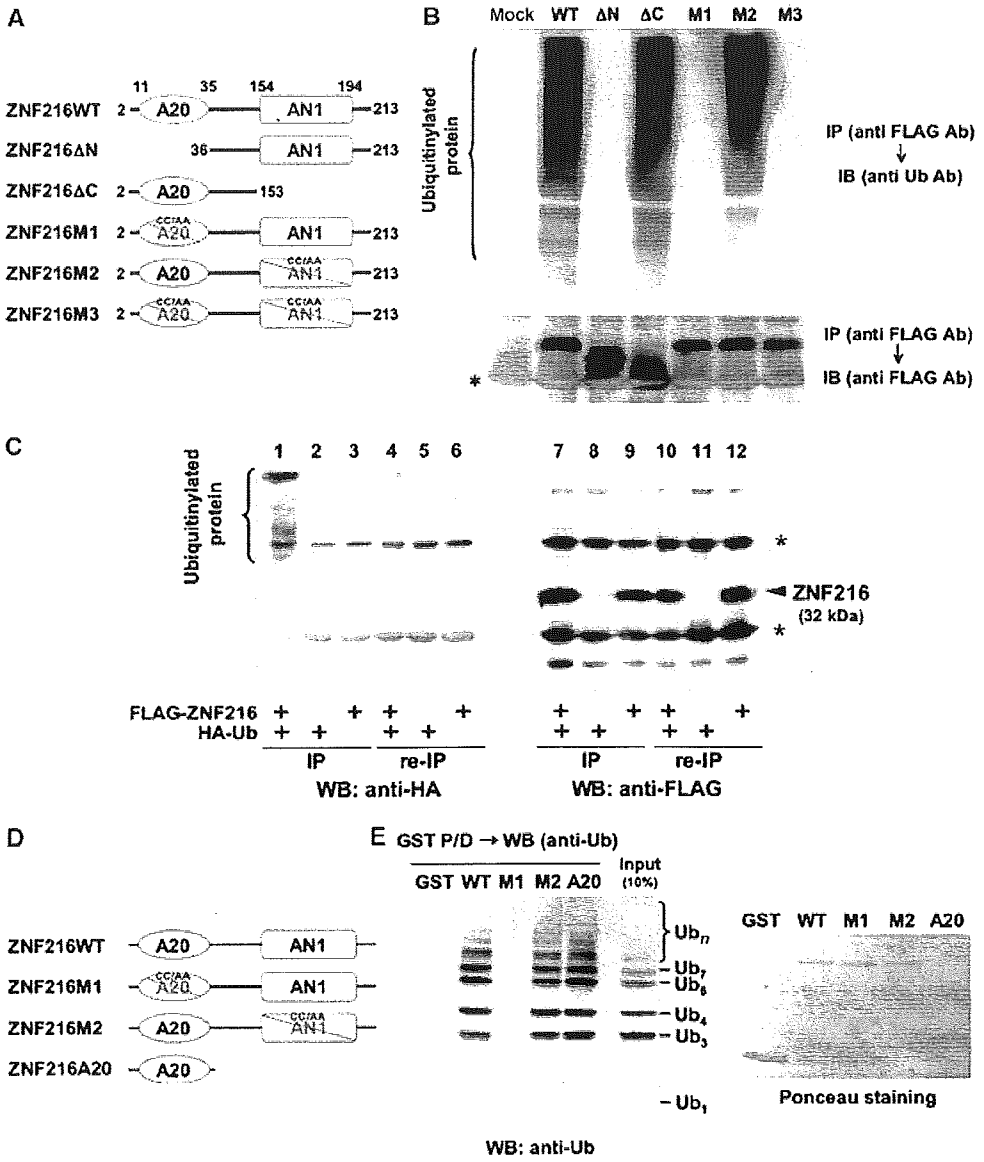

Figure 1 ZNF216 binds polyubiquitin directly through the ZnF-A20 domain. (**A**) Schematic representation of the primary structure of wild-type ZNF216 and its mutants. ZNF216ΔN (aa 36–213) and ZNF216ΔC (aa 2–153) constructs lack the ZnF-A20 (aa 11–35) and ZnF-AN1 (aa 154–194) domains, respectively. Cysteine residues at positions 30 and 33 within the ZnF-A20 were substituted with alanines (C30A/C33A) in ZNF216M1, and both cysteines 170 and 175 within the ZnF-AN1 were substituted with alanines (C170A/C175A) in ZNF216M2. Both ZnF-A20 and ZnF-AN1 domains were mutated in ZNF216M3. (**B**) Co-precipitation of ubiquitinylated proteins and ZNF216. FLAG-tagged ZNF216 or mutants were expressed in HEK293 cells, and cell extracts were immunoprecipitated with anti-FLAG antibody. Ubiquitinylated proteins detected with anti-ubiquitin antibody were precipitated with FLAG-tagged ZNF216 but not with ZnF-A20 mutants. Expression levels of FLAG-tagged ZNF216 constructs are shown at the bottom. Bands corresponding to immunoglobulin chains are marked by an asterisk. (**C**) ZNF216 is minimally ubiquitinylated. HEK293 cells expressing FLAG-tagged ZNF216 or HA-tagged ubiquitin were lysed and immunoprecipitation was performed using anti-FLAG antibody. Aliquots of precipitated beads were boiled and immunoprecipitated again (re-IP). Each sample was separated on gels and probed with anti-HA (left) or anti-FLAG antibody (right). Bands for immunoglobulin chains are marked by asterisks. (**D**) Constructs used for *in vitro* binding assay. ZNF216WT, ZNF216M1 and ZNF216 M2 were as indicated in (A). ZNF216A20 possesses only the A20 domain (aa 2–60). All constructs were produced as GST fusion proteins. (**E**) *In vitro* ubiquitin binding assay. Left panel: GST protein fused to the constructs indicated in (D) was incubated with purified K48-linked polyubiquitin chains, followed by precipitation with GSH beads. In all, 10% of purified polyubiquitin chains was separated without pull-down to evaluate protein amount (10% input). Right panel: the membrane was stained with ponceau to evaluate levels of GST fusion protein.

S2 and S3). Expression of MuRF-1 (Figure 4B) and MAFbx (Gomes *et al*, 2001) was also induced in fasting. Upregulation of *Znf216* was also observed in a model of denervation-induced muscle atrophy. Neurectomy promotes significant reduction (~20%) in the weight of gastrocnemius muscles within the first 7 days postsurgery. As expected, expression of *Znf216* and MuRF-1 was induced in gastrocnemius muscles by denervation-induced muscle atrophy (Figure 4C). These results suggest that *Znf216* expression is associated with atrophy in skeletal muscles.

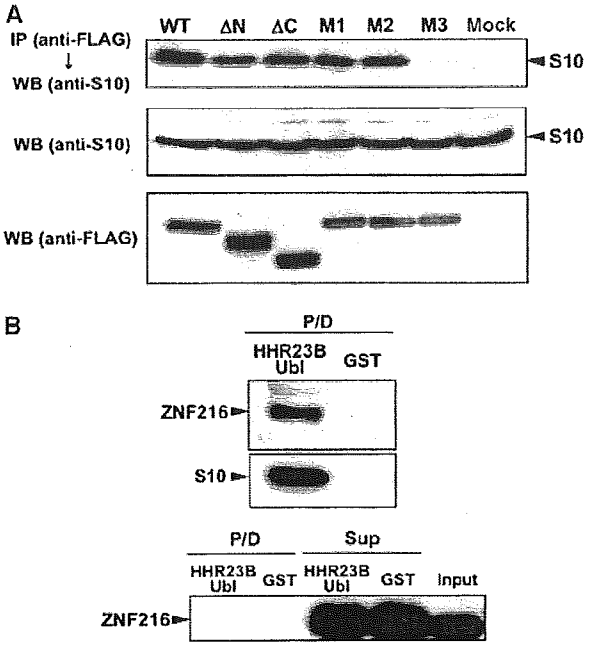

Figure 2 Interaction of ZNF216 with the 26S proteasome in mammalian cells. (**A**) Co-precipitation of the 26S proteasome and ZNF216. Co-precipitated proteins with FLAG-ZNF216 were resolved by SDS–PAGE and detected by immunoblotting using anti-S10a/Rpn7p antibody (anti-S10) or anti-FLAG antibody. Aliquots of cellular extracts were immunoblotted without immunoprecipitation to evaluate protein expression in the bottom panels. (**B**) ZNF216 was detected in the 26S proteasome fraction. Upper panel, cell lysates were incubated with a GST fusion of HHR23B Ubl (HHR23B Ubl) to isolate the 26S proteasome. Precipitated proteins (P/D) were separated and probed with anti-S10 or anti-ZNF216 antibody. Lower panel: purified recombinant ZNF216 was incubated with a GST fusion of HHR23B Ubl or GST protein. Precipitated (P/D) or not precipitated (Sup) proteins were probed with anti-ZNF216 antibody. No direct binding of ZNF216 to the Ubl domain of HHR23B was detected.

The transcription factor FOXO has been reported to play a critical role in muscular atrophy by inducing atrophy-related genes, including MAFbx/Atrogin-1 (Sandri *et al*, 2004; Stitt *et al*, 2004). Therefore, we asked whether FOXO activation upregulated *Znf216* expression. To do so, we employed a Cre-loxP system (Furukawa-Hibi *et al*, 2002) in which constitutively active FOXO4 (AFX-TM) created by mutation of the three Akt phosphorylation sites, T32A, S253A and S315A (Brunet *et al*, 1999), was expressed in C2C12-AFX-TM cells following infection by Cre recombinase-expressing adenovirus (Cre) (Figure 4D). Both AFX-TM mRNA and protein were induced 24 h after infection with Cre but not with control adenovirus (Furukawa-Hibi *et al*, 2002). ZNF216 mRNA was markedly increased in C2C12-AFX-TM cells as a result of infection with Cre but not following infection with control virus (Figure 4E). These results suggest that ZNF216 may function as a downstream effector of FOXO in muscle atrophy.

Generation of mice lacking ZNF216

To investigate the *in vivo* function of ZNF216, mice deficient for ZNF216 ($Znf216^{lex/lex}$) were generated by gene trapping at Omnibank of Lexicon Genetics (Zambrowicz *et al*, 1998). The structure of the predicted trapped gene is shown in Figure 5A. The trapping vector, VICTR48, was inserted 3.3 kbp upstream of exon 3, which encodes the first methionine of mouse *Znf216* (Figure 5A). $Znf216^{lex/lex}$ mice were born from interbred heterozygous $Znf216^{+/lex}$ mice in Mendelian ratios, indicating that ZNF216 is dispensable for embryogenesis or fetal development. No ZNF216 mRNA or protein was detected in $Znf216^{lex/lex}$ mice by Northern or immunoblot analyses, respectively (Figures 5B and C), indicating that the mice are ZNF216 nulls. Expression levels of ZNF216 in $Znf216^{+/lex}$ heterozygotes were nearly one-half those of wild-type mice. $Znf216^{lex/lex}$ mice were viable and fertile, without gross abnormalities or apparent pathological alteration, but they weighed less than sex- and age-matched controls (Figure 5D). At 45 weeks, the average weights of $Znf216^{+/+}$ and

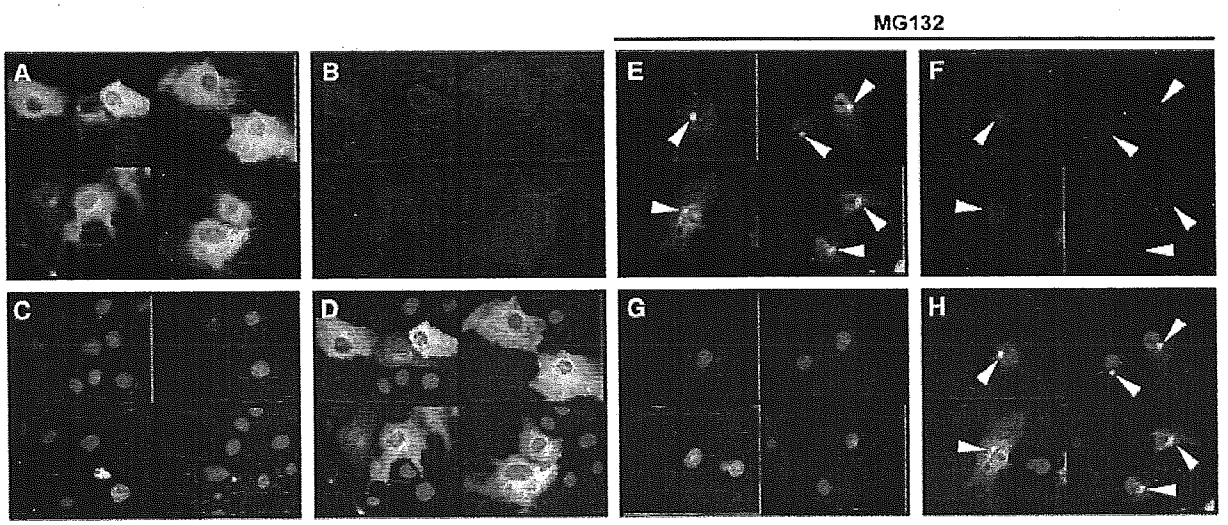

Figure 3 ZNF216 is localized in 'aggresomes' with ubiquitinylated proteins. (**A–H**) COS cells were transfected with expression vectors for FLAG-tagged ZNF216 and HA-tagged ubiquitin. Fixed cells were subjected to indirect immunofluorescence using (A, E) anti-FLAG (with AlexaFluor 488 anti-mouse IgG, green) and (B, F) anti-HA (with AlexaFluor 546 anti-rat IgG antibodies, red) antibodies. (C, G) Nuclei were stained with DAPI in the same fields of each panel. (E–H) Transfected COS cells were treated with the proteasome inhibitor, MG132 (0.5 μM). Aggresomes formed are indicated by arrowheads. The merged images were shown in (D and H).

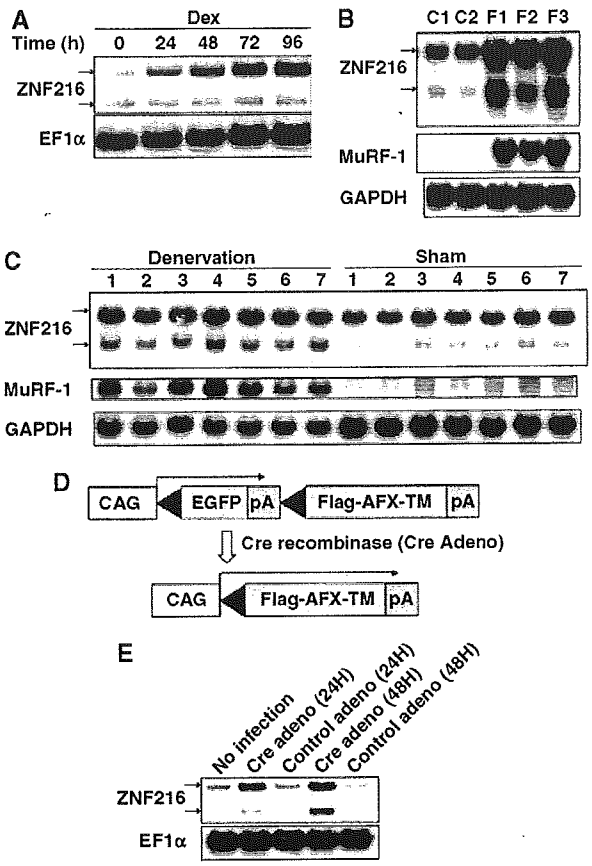

Figure 4 Expression of ZNF216 is induced by muscle atrophy. (**A**) C2C12 myoblast cells were differentiated into myotubes, and treated with 100 μM Dex for the indicated times. Northern blotting was performed to reveal the effect of Dex on ZNF216 expression. The entire coding region of ZNF216 was used as a probe, which recognized 2.4 and 1.5 kb mRNA species arising from alternative splicing and polyadenylation. The loading control was elongation factor α (EF1α). (**B**) Fasting-induced muscle atrophy. Three mice were fasted (F1∼F3), and two mice (C1, C2) were fed freely. After 2 days, RNA was purified from gastrocnemius muscle, and Northern blotting was performed to determine ZNF216 expression. The membrane was re-probed with MuRF-1 and GAPDH. (**C**) Denervation-induced muscle atrophy was induced by cutting the sciatic nerve of the hindlimb of seven mice (1∼7). The opposite limb was sham operated as the control. At 7 days after surgery, total RNA was purified from gastrocnemius muscles, and Northern blotting was performed to detect ZNF216 expression. The membrane was re-probed with MuRF-1 and GAPDH. (**D**) Cre-loxP-mediated, constitutively active FOXO expression system. cDNA encoding FLAG-tagged constitutively active FOXO4 (AFX-TM) is separated from the CAG promoter of an expression vector by a loxP-flanked EGFP-poly(A) cassette. Infection with adenovirus expressing Cre recombinase (Cre) results in excision of the DNA fragment located between the two loxP sequences and expression of FLAG-tagged AFX-TM. (**E**) ZNF216 is downstream of FOXO. Total RNAs were prepared from C2C12-AFX-TM cells at the indicated times after infection with adenovirus expressing Cre (Cre) or lacZ (control) and probed by *Znf216* or EF1α. A marked increase in expression of *Znf216* was observed only in Cre-infected cells.

Znf216$^{lex/lex}$ male mice were 42.66±7.06 g (n=14) and 33.16±4.44 g (n=9), respectively. The average weights of female *Znf216*$^{+/+}$ and *Znf216*$^{lex/lex}$ mice were 34.46±4.21 g (n=14) and 26.85±5.38 g (n=11), respectively. After 30 weeks, both female and male *Znf216*$^{lex/lex}$ mice showed no or subtle increases in weight, whereas *Znf216*$^{+/+}$ or

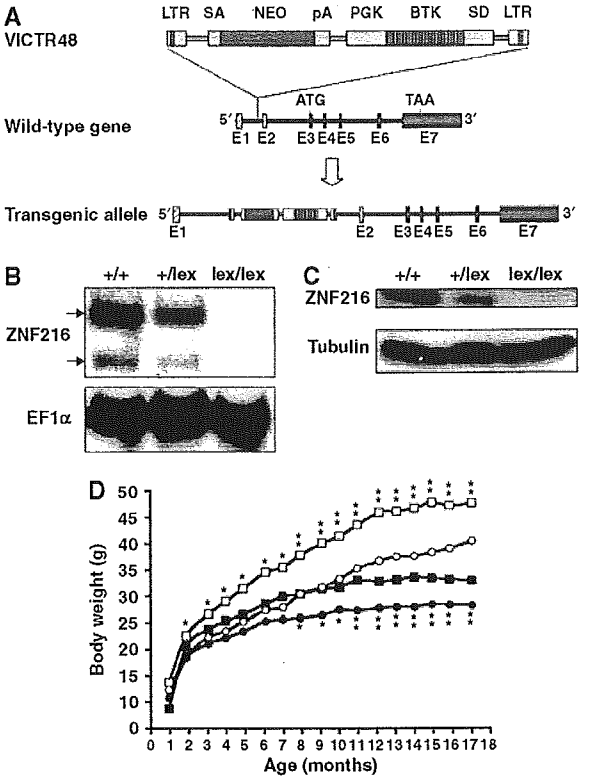

Figure 5 Disruption of *Znf216* gene in mice. (**A**) Gene trap strategy of *Znf216* gene. The structure of the trapping vector, VICTR48, is shown in the upper line. The wild-type allele and the trapped, transgenic allele follow the vector. The retroviral vector, VICTR48, was integrated between exons 1 and 2 of the *Znf216* gene and transcription of downstream exons encoding ZNF216 was diminished. Exons are depicted by striped (noncoding exons) or shadowed boxes (protein-coding exons) and numbered (E1 and E2). LTR, long terminal repeat; SA, splice acceptor site; SD, splice donor site; pA, polyadenylation signal; PGK, PGK promoter. (**B**) Northern blot analysis. Total RNA was prepared from brains of *Znf216*$^{+/+}$, *ZnfF216*$^{+/lex}$ or *Znf216*$^{lex/lex}$ mice. Full-length mouse ZNF216 cDNA was used as a probe. The membrane was re-probed using an EF1α probe. (**C**) Immunoblot analysis. Extracts from brain of *Znf216*$^{+/+}$, *Znf216*$^{+/lex}$ or *Znf216*$^{lex/lex}$ mice were immunoblotted with antibody against ZNF216. The membrane was re-probed using anti-tubulin antibody. (**D**) Growth curve of *Znf216*$^{lex/lex}$ mice. Body weights at each time point of *Znf216*$^{+/+}$ and *Znf216*$^{lex/lex}$ mice were indicated as open square boxes (males) or circles (females) and closed square boxes (males) or circles (females), respectively. $^{*}P<0.05$; $^{**}P<0.005$.

Znf216$^{+/lex}$ mice gained weight as they aged (Figure 5D). The size of most organs in *Znf216*$^{lex/lex}$ mice was reduced in proportion with body weight. However, the fat volume of aged (>30 weeks of age) *Znf216*$^{lex/lex}$ mice was significantly decreased, suggesting that the marked difference in body weight between wild-type and aged *Znf216*$^{lex/lex}$ mice is mainly caused by decreased fat mass seen in *Znf216*$^{lex/lex}$ mice (not shown). Detailed phenotypic characterization of aged mutant mice will be provided elsewhere.

Znf216$^{lex/lex}$ mice exhibit partial resistance to denervation-induced muscle atrophy

To further explore the involvement of ZNF216 in muscle atrophy, neurectomy of sciatic nerve was undertaken in wild-type and *Znf216*$^{lex/lex}$ mice. As shown in Figure 6A, 7

days after denervation, significant muscle weight loss and reduction in fiber sizes of the gastrocnemius muscle were observed in wild-type mice. By contrast, such decreases in muscle weight were significantly attenuated in *Znf216*$^{lex/lex}$ mice (Figure 6A). Sections of gastrocnemius muscle also showed larger fibers in muscle from neurectomized *Znf216*$^{lex/lex}$ mice than in control muscle (Figure 6B). However, there was no significant difference in fiber area between sham-operated wild-type and *Znf216*$^{lex/lex}$ mice (wild type + sham operated, $1988 \pm 530\,\mu m^2$; wild type + denervation, $1379 \pm 345\,\mu m^2$; lex/lex + sham operated, $1776 \pm 484\,\mu m^2$; lex/lex + denervation, $1393 \pm 344\,\mu m^2$). As shown in Figure 6C, the reduction in fiber area was also less apparent in *Znf216*$^{lex/lex}$ mice compared to wild-type mice. These results suggest that ZNF216 plays a crucial role in reduction of muscle mass on denervation-induced muscle atrophy.

Abnormal accumulation of ubiquitinylated proteins in muscle from Znf216$^{lex/lex}$ mice

To investigate what abnormalities occur during denervation-induced muscle atrophy in *Znf216*$^{lex/lex}$ mice, we examined expression levels of factors involved in muscle atrophy. As expected, expression of MAFbx/Atrogin-1 and MuRF-1 was dramatically induced by denervation-induced muscle atrophy in gastrocnemius muscle from wild-type mice (Figure 6A). In *Znf216*$^{lex/lex}$ mice, expression of MAFbx/Atrogin-1 and MuRF-1 was also induced at levels comparable to those seen in wild-type mice. Induction of *Pmsa1* and *Pmsd11*, genes encoding the 26S proteasome subunits α6 and Rpn6, respectively, was also indistinguishable between *Znf216*$^{lex/lex}$ and wild-type mice (Figure 7A). Furthermore, proteasome activities in gastrocnemius muscles were comparable between wild-type and *Znf216*$^{lex/lex}$ mice (Figure 7B). Thus, induction of relevant ubiquitin ligases or proteasome components was not affected in *Znf216*$^{lex/lex}$ mice. It is known that ubiquitinylated proteins accumulate during muscle atrophy (Medina *et al*, 1991; Wing *et al*, 1995). As shown in Figure 7C, following denervation, ubiquitinylated proteins accumulated in the gastrocnemius muscle of wild-type mice, but higher levels of ubiquitinylated proteins accumulated in muscle derived from *Znf216*$^{lex/lex}$ mice (~2-fold: $P<0.001$ in neurectomized *Znf216*$^{lex/lex}$ versus wild-type muscle). Similar results were obtained by fasting-induced muscle atrophy, although no difference in the levels of ubiquitinylated proteins from controls (sham-operated or fed) was observed between genotypes (Figure 7C). These results indicate that ZNF216 is a critical regulator of muscle atrophy, most likely functioning to regulate degradation of muscle proteins without altering expression of proteasomal components or known E3 ligases.

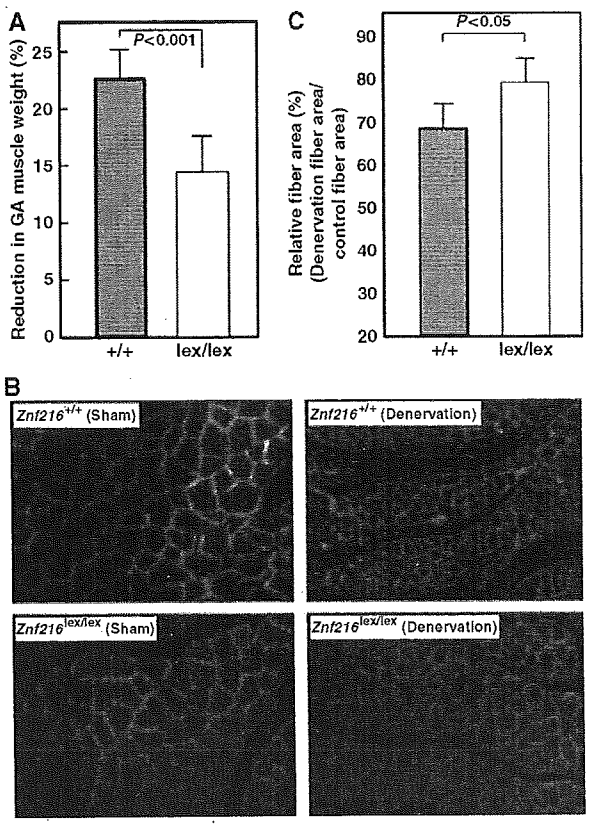

Figure 6 Denervation induced muscular atrophy was attenuated in *ZNF216*$^{lex/lex}$ mice. (**A**) Reduction of GA muscle weight upon neurectomy. Percent decreases in muscle weights are shown as a percent of control, calculated as the left/right muscle weights. (**B**) Cross-sections from gastrocnemius muscle were stained by indirect immunofluorescence with anti-laminin. The reduction in size was also significant in muscle fibers of control mice but less in *Znf216*$^{lex/lex}$. (**C**) Muscle fiber cross-sectional areas were measured in transverse tissue section (B). Percent relative fiber area of denervated muscle to control fiber area (sham-operated) are shown.

Effect of ZNF216 on UPS-mediated protein degradation

Accumulation of ubiquitinylated protein under any circumstance might be because of loss of inhibition of ubiquitinylation and/or deubiquitinylation (DUB). However, no inhibition or DUB activity was observed (Supplementary Figures S4 and S5). As shown in Figure 7D, association of ZNF216 protein to the proteasome was significantly increased when atrophy was induced, suggesting that ZNF216 may be involved in association of ubiquitinylated proteins and the proteasome. The biochemical activity of ZNF216 is similar to that of the UPS proteins, hHR23 and hPLIC, both of which have a shuttle function and are known to bind to both polyubiquitinylated proteins and the 26S proteasome (Hartmann-Petersen and Gordon, 2004; Elsasser and Finley, 2005). Interestingly, overexpression of hHR23 and hPLIC results in stabilization of unstable proteins such as p53 (Kleijnen *et al*, 2000; Glockzin *et al*, 2003). To determine if ZNF216 functioned similarly, we employed a degradation system using unstable GFP (Bence *et al*, 2001). In this system, the CL1 peptide, which functions as a degron, is fused to EGFP (EGFP-CL1). Degradation by conjugation with the degron is mediated by the UPS (Bence *et al*, 2001). EGFP-CL1, constitutively expressed in HEK293 cells, is unstable and the estimated half-life ($t_{1/2}$) of EGFP-CL1 in this system is about 11 min. Ubiquitinylated EGFP-CL1 protein stabilized by treatment with a proteasome inhibitor was associated with ZNF216 but EGFP itself was not (not shown). As shown in Figure 8A, protein degradation was markedly retarded in the presence of ectopic ZNF216 ($t_{1/2}>30$ min) compared to cells transfected with the loss of function mutant ZNF216M3 or mock-transfected cells. Rapid turnover of EGFP-CL1 protein was inhibited by treatment with the

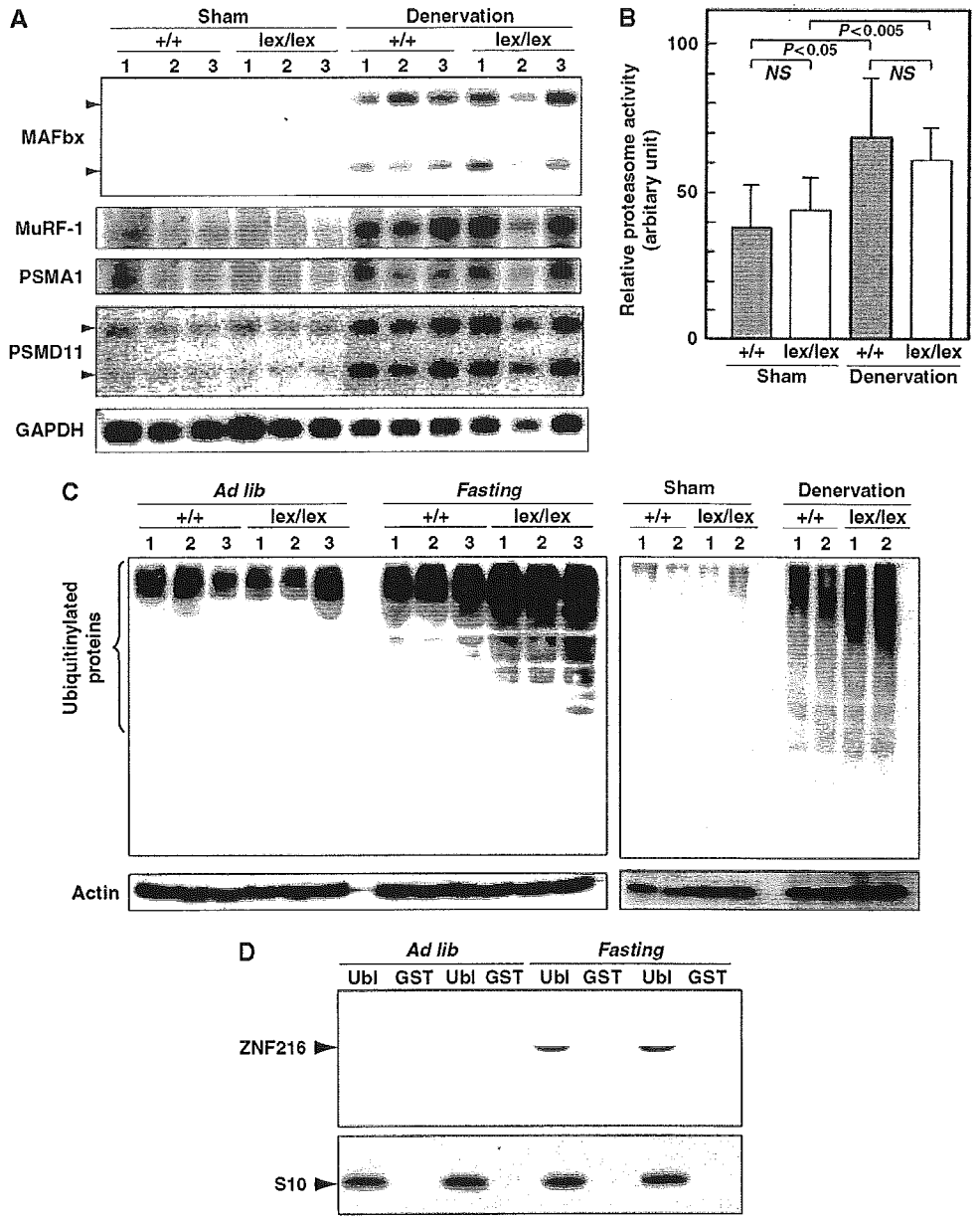

Figure 7 Changes in UPS upon muscular atrophy. (**A**) Expression of UPS components in denervation-induced muscular atrophy. Total RNAs were purified from gastrocnemius muscle, and Northern blotting was performed using indicated probes. Expression of genes for ubiquitin-ligases, such as MAFbx or MuRF-1, and proteasome subunits PSMA1 and PSMD11 was induced by muscle atrophy at comparable levels between wild-type and *ZNF216*$^{lex/lex}$ mice. (**B**) Proteasome activity. Proteasome activities in muscle extracts from wild-type or *ZNF216*$^{lex/lex}$ mice were measured and are shown as arbitrary units. No significant difference in proteasome activity between wild-type and *ZNF216*$^{lex/lex}$ was observed. (**C**) High levels of ubiquitinylated proteins accumulated in muscles from *ZNF216*$^{lex/lex}$ mice than in muscles from wild-type mice. Muscle extracts from wild-type or *ZNF216*$^{lex/lex}$ mice were subjected to immunoblotting using anti-ubiquitin antibody to analyze levels of ubiquitinylated proteins. Left and right panels show fasting-induced and denervation-induced muscle atrophy, respectively. Each membrane was re-probed with anti-actin antibody. (**D**) Association of ZNF216 with the proteasome was increased upon atrophy. The proteasome fractions in muscle extracts from fed (*ad lib*) or fasted (fasting) mice were precipitated with GST-Ubl or GST only as a negative control. Endogenous ZNF216 protein was co-precipitated with the proteasome, which is probed by the anti-S10 antibody.

proteasome inhibitor MG132 (MG132, Figure 8B). The levels of the proteins stabilized by MG132 were comparable among cells transfected with ZNF216 constructs, indicating that protein synthesis of EGFP-CL1 was not significantly affected by ectopic expression of ZNF216 (MG132, Figure 8B). ZNF216WT, and to a lesser extent the mutants M1 and M2 but not M3, attenuated degradation (NT, Figure 8B). Thus, as is the case with other shuttle proteins, overexpression of ZNF216 inhibits degradation of unstable proteins via the UPS.

Discussion

ZNF216 is an atrogene

In this report, we show that *Znf216*$^{lex/lex}$ mice exhibit resistance to denervation-induced muscle atrophy. It has been

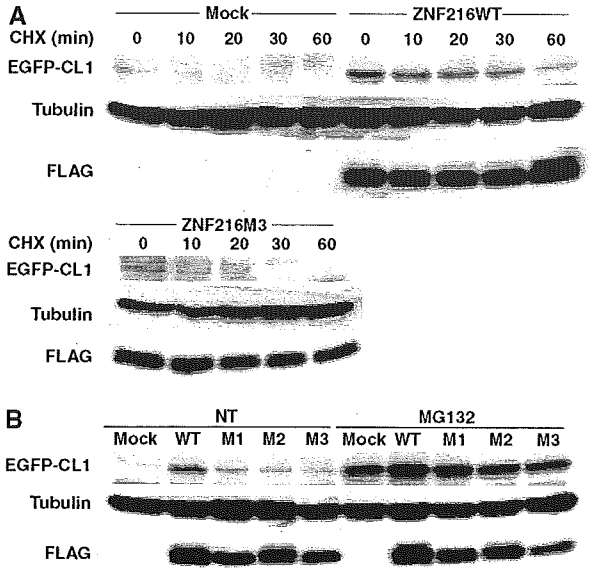

Figure 8 Ectopic expression of ZNF216-affected protein degradation. (**A**) Degradation of EGFP-CL1 protein was delayed by overexpression of ZNF216. 293 cells stably expressing EGFP-CL1 were transfected with plasmid of ZNF216WT, ZNF216M3 or pcDNA3 (mock). Estimated half-lives of the EGFP-CL1 are 35, 11 and 11 min in ZNF216WT-, ZNF216M3- and mock-transfected cells, respectively. *De novo* protein synthesis was arrested by cycloheximide (CHX). The membrane was re-probed with tubulin antibody to control for protein loading (tubulin) and FLAG antibody to detect ZNF216 expression (FLAG). (**B**) Degradation of EGFP-CL1 protein in the presence of various ZNF216 constructs. HEK293 cells stably expressing EGFP-CL1 were transfected with plasmids expressing the indicated mutants. Transfected cells were not treated (NT) or MG132-treated (MG132), and EGFP-CL1 protein was detected with an anti-GFP antibody (EGFP-CL1). The membrane was re-probed with tubulin antibody to control for protein loading (tubulin) and FLAG antibody to detect ZNF216 expression (FLAG).

shown that TNFα induces catabolic conditions through UPS during cancer cachexia (Mitch and Price, 2001). Recently, it has been reported that mice deficient in molecules involved in the NF-κB pathway exhibit resistance to muscular atrophy (Cai *et al*, 2004; Hunter and Kandarian, 2004; McKinnell and Rudnicki, 2004). On the other hand, the IGF-FOXO axis has been suggested to regulate muscle mass through induction of 'atrogenes' such as Murf1 and MAFbx/Atrogin-1 (Sandri *et al*, 2004; Stitt *et al*, 2004). Although we provide evidence that *Znf216* is downstream of FOXO, the NF-κB pathway could represent an alternative signal inducing ZNF216. Indeed, we have identified *Znf216* as a gene induced by RANKL, a TNF family ligand (Hishiya *et al*, 2005) which activates the NF-κB pathway through RANK (Anderson *et al*, 1997; Lacey *et al*, 1998). Moreover, TNFα and IL-1β upregulate expression of ZNF216 in fibroblasts and macrophages (Hishiya *et al*, 2005). These results suggest that *Znf216* may be activated by NF-κB. Huang *et al* (2004) recently reported that ZNF216 inhibits the NF-κB pathway. Whereas treatment with TNFα or overexpression of TRAF6 dramatically activated a reporter driven by NF-κB response elements, ectopic expression of A20/TNFAIP3 but not ZNF216 inhibited NF-κB activation (not shown). Using mouse embryonic fibroblasts, splenocytes or bone marrow cells from $Znf216^{lex/lex}$ or wild-type mice, no significant differences were observed in TNFα-dependent NF-κB activation, LPS-induced cytokine expression or proliferation (unpublished data). Therefore, ZNF216 seems to function as a downstream effector (i.e., a component of the UPS) rather than a specific negative regulator of NF-κB signaling, although ZNF216 function in that pathway is still under investigation. Whereas expression of ZNF216 is not restricted to muscle, such expression was induced upon muscular atrophy and loss of function of *Znf216* promotes resistance to denervation-induced atrophy, thereby suggesting that it fulfills the definition of an 'atrogene'.

As it is in skeletal muscle, ZNF216 is highly expressed in the brain (Scott *et al*, 1998). Aberrations in the UPS have been documented in the pathogenesis of neurodegenerative diseases such as Parkinson's and Huntington's diseases (Ross and Poirier, 2004). Massive accumulation of ubiquitinylated proteins, which are often aggregated and impair the UPS leading to neuronal degeneration, has been observed in these pathogenic conditions (Ciechanover and Brundin, 2003; Korhonen and Lindholm, 2004). In cultured cells, blocking the UPS by proteasome inhibitors leads to accumulation of ubiquitinylated proteins. These ubiquitinylated proteins are then transferred to perinuclear locations and form aggresomes (Johnston *et al*, 1998). As shown here, ZNF216 is localized in aggresomes together with ubiquitinylated proteins. Interestingly, proteomic analysis of a protein complex containing HDAC6, a protein often associated with aggresomes (Kawaguchi *et al*, 2003), showed that the complex included AWP1, a structural homologue of ZNF216 (Seigneurin-Berny *et al*, 2001). Although it is unclear whether ZNF216 is involved in aggresome formation, there is great interest in the role of ZNF216 in the pathogenesis of neurodegenerative diseases.

Molecular function of an A20-containing protein, ZNF216

In muscle atrophy, more ubiquitinylated proteins accumulate in muscle from $Znf216^{lex/lex}$ mice than in muscle from wild-type mice, suggesting an abnormal UPS function. Inhibition of neither polyubiquitinylation nor DUB activity was observed in ZNF216. Although our *in vivo* data showed significant accumulation of polyubiquitinylated proteins in muscle from $Znf216^{lex/lex}$ mice, there is a possibility that ZNF216 is a ubiquitin-ligase. It has been recently reported that A20/TNFAIP3 protein possesses ubiquitin ligase activity against RIP through its ZnF-A20 repeats (Wertz *et al*, 2004). We asked whether the ZnF-A20 of ZNF216 exhibited activity similar to A20/TNFAIP3, but *in vitro* ubiquitinylation assays were negative (Supplementary Figure S6). In fact, the ZnF-A20 of A20/TNFAIP3 protein does not bind polyubiquitin chains as does the ZnF-A20 of ZNF216 (Supplementary Figure S1). Furthermore, there are seven ZnF-A20 motifs in A20/TNFAIP3 and only the fourth is responsible for E3 activity, suggesting that the ZnF-A20 motif is not inherently active enzymatically (Wertz *et al*, 2004). However, we cannot exclude the possibility that ZNF216 may possess DUB or E3 activity highly specific to an unknown substrate without nonspecific or self-ubiquitinylating activity.

ZNF216 likely acts as a bridging or a shuttle factor of ubiquitinylated proteins targeted to the proteasome. Shuttle proteins, such as Rad23p and Dsk2p, share interfaces for ubiquitinylated proteins and the proteasome (Hartmann-Petersen and Gordon, 2004; Elsasser and Finley, 2005).

Although shuttle proteins are required for efficient protein degradation, ectopic expression of hHR23 or hPLIC, the human homologues of Rad23p or Dsk2p, respectively, lead to stabilization of p53 protein (Kleijnen *et al*, 2000; Glockzin *et al*, 2003). These outcomes may be caused by titration effects due to overexpression and are commonly observed following misexpression of shuttle proteins in yeast and mammals (Hartmann-Petersen and Gordon, 2004; Verma *et al*, 2004). Here, we show that ZNF216 has a ubiquitin binding domain and can associate with the 26S proteasome even in the absence of ubiquitin binding, and that overexpression of the zinc-finger protein attenuates protein degradation rate. There is no structural counterpart of ZNF216 in the yeast genome. We asked whether ZNF216 could rescue the bridging function of RAD23 or DSK2 mutants by introducing ZNF216 into *Δrad23Δdsk2* yeast cells, but the phenotype could not be rescued (data not shown). This suggests that ZNF216 is not the functional orthologue of these proteins. Recently, the presence of an alternative pathway of Rad23p/Dsk2p in protein targeting to the proteasome has been suggested (Bazirgan and Hampton, 2005; Richly *et al*, 2005). It has been reported that tetra-ubiquitin constitutes the minimum proteasomal targeting signal and that the length of polyubiquitin chain may determine the targeting route (Thrower *et al*, 2000; Bazirgan and Hampton, 2005; Richly *et al*, 2005). Notably, ZNF216 preferentially binds polyubiquitin chains longer than di- or tri-ubiquitin (Figure 1D). Therefore, these data suggest that ZNF216 is a novel ubiquitin recognition factor, required for efficient protein degradation via a pathway different from the canonical Rad23p/Dsk2p pathway. Although it is now under investigation, the characterization of ZnF-AN1, an AN1-type zinc-finger domain located at the C-terminus of ZNF216, may reveal the precise molecular function of ZNF216.

Materials and methods

Antibodies

An anti-ZNF216 antibody was raised by immunizing rabbits against synthesized peptide corresponding to the C-terminal sequence of mouse ZNF216. Mouse monoclonal antibodies for FLAG (Sigma, St Louis, MO) and ubiquitin (Santa Cruz Biotechnology, CA), rabbit polyclonal antibodies for ubiquitin (Affiniti Research Products) and actin (Neo Markers, CA), a rat monoclonal antibody for HA (Roche Diagnostics, Mannheim, Germany), and a rabbit polyclonal antibody against S10a/Rpn7p (Affiniti Research Products) were purchased from the indicated manufacturers. For indirect immunofluorescence staining, AlexaFluor 488 goat anti-mouse IgG or AlexaFluor 546 goat anti-rat IgG antibody was obtained from Molecular Probes, OR.

Identification of interacting proteins

RNA was purified from RAW264.7 cells stimulated by RANKL, and used to construct the yeast library (MatchMaker Library Construction & Screening Kit, Clontech). Yeast two-hybrid screening with pGBKT7-ZNF216 was performed as described previously (Masuda *et al*, 2001). Identification of the co-immunoprecipitated proteins with N- or C-terminally FLAG-tagged ZNF216 (ZA20D2) or AWP1 (ZA20D3) was essentially done by a nano-LC/MS/MS system as previously described (Natsume *et al*, 2002; Komatsu *et al*, 2004).

Experimental models of muscle atrophy

For fasting-induced muscle atrophy, 8-week-old C57BL6 male mice were deprived of food but given free access to water. After 2 days, gastrocnemius muscles were harvested for each experiment. Denervation-induced muscle atrophy was performed by dissecting the sciatic nerve of one hindlimb, and the other hindlimb was sham operated as the control. After 7 days, the contralateral normal and denervated gastrocnemius muscles were harvested for each experiment. All animal experiments were approved in advance by the Ethics Review Committee for Animal Experimentation of the National Institute for Longevity Sciences and the National Center for Geriatrics and Gerontology. Student's *t*-tests were used to evaluate statistical differences between the two groups.

Znf216-deficient mice

Generation of heterozygous *Znf216*$^{+/lex}$ mice was essentially done by the gene trap method at Lexicon Genetics (Zambrowicz *et al*, 1998). Briefly, ES cells heterozygous for the trapped *Znf216* gene were microinjected into eight-cell-stage ICR mouse embryos and transplanted into uteri. Chimeric mice were crossed to C57BL/6J mice. Northern and immunoblot analyses confirmed disruption of the gene (see text). For genotyping, primers were as follows: KO-A, ACCGACAGGATAGACAATGGCAGAG; KO-B, CGATTTTAAGAAAG GAGGCTCTGACC; LTR2, AAATGGCGTTACTTAAGCTAGCTTGC. The wild-type and inserted alleles were detected by PCR using KO-A and KO-B (0.5 kb), and LTR2 and KO-B (0.3 kb), respectively.

EGFP-CL1 degradation assay

The nucleotide sequence encoding the CL1 peptide (ACKNWFSSLSHFVIHL) (Gilon *et al*, 1998) was inserted into the *Xho*I/*Eco*RI site of pEGFP-C3, and the resulting plasmid was designated pEGFP-CL1. A cell line stably expressing EGFP-CL1 (293EGFP-CL1) was generated by transfection of pEGFP-CL1 into 293 cells. For the degradation assay, ZNF216 expression vectors were transfected into 293EGFP-CL1 cells and cells were harvested 48 h after transfection. MG132 (final 10 μM) or cycloheximide (final 100 μg/ml) was added to the culture at 12 or 1 h before harvest, respectively. Protein extraction was as described above.

For more details on supplementary Materials and methods, see Supplementary data

Supplementary data

Supplementary data are available at *The EMBO Journal* Online.

Acknowledgements

We are grateful to Drs Kazuhiro Iwai (Osaka City University) and Noboru Motoyama (NCGG) for reagents, helpful comments and suggestions throughout this study. We also thank Drs Akio Matsuda and Tatsuo Furuyama for experimental instruction and advice; Dr Aya Sasaki for pathological determinations; Ms Miho Kamiya and Ms Kumi Tsutsumi for technical assistance; and Dr Elise Lamar for proofreading the manuscript. This study is supported in part by the Program for Promotion of Fundamental Studies in Health Sciences of the Organization for Pharmaceutical Safety and Research of Japan, and by a Research Grant for Longevity Sciences from the Ministry of Health, Labor and Welfare.

References

Anderson DM, Maraskovsky E, Billingsley WL, Dougall WC, Tometsko ME, Roux ER, Teepe MC, DuBose RF, Cosman D, Galibert L (1997) A homologue of the TNF receptor and its ligand enhance T-cell growth and dendritic-cell function. *Nature* **390**: 175–179

Bailey JL, Wang X, England BK, Price SR, Ding X, Mitch WE (1996) The acidosis of chronic renal failure activates muscle proteolysis in rats by augmenting transcription of genes encoding proteins of the ATP-dependent ubiquitin-proteasome pathway. *J Clin Invest* **97**: 1447–1453

Bazirgan OA, Hampton RY (2005) Cdc48-Ufd2-Rad23: the road less ubiquitinated? *Nat Cell Biol* **7**: 207–209

Bence NF, Sampat RM, Kopito RR (2001) Impairment of the ubiquitin–proteasome system by protein aggregation. *Science* **292**: 1552–1555